# Bioclimatic change as a function of global warming from CMIP6 climate projections

Morgan Sparey[1], Peter Cox[1], and Mark S. Williamson[1,2]

[1]Mathematics and Statistics, Faculty of Environment, Science and Economy, University of Exeter, Exeter, EX4 4QF, UK
[2]Global Systems Institute, University of Exeter, Exeter, EX4 4QE, UK

**Correspondence:** Morgan Sparey (ms959@exeter.ac.uk)

**Abstract.** Climate change is predicted to lead to major changes in terrestrial ecosystems ~~(Pörtner et al., 2022)~~. However, ~~significant~~ substantial differences in climate model projections for given scenarios of greenhouse gas emissions ~~(Masson-Delmotte et al., 202~~ , continue to ~~hinder~~ limit detailed assessment. Here we show, using a traditional Köppen-Geiger bioclimate classification system ~~(Köppen, 1884)~~, that the latest CMIP6 Earth System Models actually agree ~~very~~ well on the fraction of the global land-surface that ~~will undergo a significant~~ would undergo a major change per degree of global warming. Data from 'historical' and 'ssp585' model runs are used to create bioclimate maps at various degrees of global warming, and to investigate the performance of the multi-model ensemble mean when classifying climate data into discrete categories. Using a streamlined Köppen-Geiger scheme with 13 classifications, global bioclimate classification maps at 2K and 4K of global warming above a 1901 - 1931 reference period are presented. These projections show large shifts in bioclimate distribution, with an almost exclusive change from colder, wetter bioclimates to hotter, dryer ones. Historical model run performance is assessed and examined by comparison with the bioclimatic classifications derived from the observed climate over the same time period. The fraction ($f$) of the land experiencing a change in its bioclimatic class as a function of global warming ($\Delta T$) is estimated by combining the results from the individual models. Despite the discrete nature of the bioclimatic classification scheme, we find only a weakly-saturating dependence of this fraction on global warming ~~$f = 1 - e^{-0.17\Delta T}$~~ $f = 1 - e^{-0.14\Delta T}$, which implies about ~~12~~13% of land experiencing a ~~significant~~ major change in climate, per 1K increase in global mean temperature between the global warming levels of 1 and 3K. Therefore, we estimate that stabilising the climate at 1.5K rather than 2K of global warming, would save over ~~7~~7.5 million square kilometres of land from a major bioclimatic change.

## 1 Introduction

Understanding the impacts that climate change will have at a regional level yields vital information for adaptation to climate change. Furthermore, quantifying the performance of climate models is important for the continued improvement of climate models, and for understanding the ~~regional~~ areas where particular models under perform. There are substantial differences in climate model projections for given scenarios of greenhouse gas emissions (Masson-Delmotte et al., 2021). Climate change is predicted to lead to major changes in terrestrial ecosystems (Pörtner et al., 2022).

Here we use the Köppen-Geiger (KG) bioclimate classification to examine and quantify changes in biome under various levels of projected future global warming within the Coupled Model Intercomparison Project phase 6 (CMIP6) climate models ~~. We examine the differences between climate projections in terms of traditional KG classifications which summarise the aspects of regional climates which are most relevant to biomes, and therefore to the impacts~~ (Eyring et al., 2016). CMIP6 is an international collaboration to run a standardised set of potential future scenarios with a range of climate models developed at various institutions. The results make a compelling case for the need to further prioritise climate change mitigation policies. However, this may not be immediately clear to public or policy makers. Improved understanding of the consequences of climate change ~~on the natural environment. To remove the zeroth order uncertainty that arises from different climate model sensitivities to radiative forcing (Sherwood et al., 2020; Nijsse et al., 2020), and to make our results relevant to the Paris climate targets, we look specifically at changes in KG classification at different levels of global warming (1.5K, 2K, and 4K). A streamlined KG scheme is also implemented to visually demonstrate the impacts of warming on global biome distribution.~~ is needed, and climate classification schemes can help in that respect.

~~Climate~~ The biome of a region is largely dictated by that region's climate. Bioclimates are defined by the preferences of living organisms. Bioclimate classification empirically separates regions of the globe based on climate data and the geographical distribution of biomes. The KG bioclimate classification scheme is one of the most established, first developed by Wladimir ~~Koppen~~ Köppen (Köppen, 1884) and then enhanced by Rudolf Geiger. The original KG classification scheme consists of thirty separate bioclimates based on dominant vegetation as type determined by Köppen's experience as a botanist. These classifications are based on monthly average temperature and precipitation at each location. The seasonality of these variables, combined with threshold values, determines the bioclimate classification of the region (Peel et al., 2007).

~~CMIP6 is an international collaboration to run a standardised set of potential future scenarios with a range of climate models developed at various institutions. The results make a compelling case for the need to further prioritise climate change mitigation policies. However, this may not be immediately clear to public or policy makers. Improved understanding of the consequences of climate change is needed, and climate classification schemes can help in that respect~~Classifications include hot and cold deserts - regions where there is no rainfall, and tropical rainforests - regions where minimum temperature and threshold precipitation is met.

Bioclimate classification systems, such as the KG and Holdridge schemes (Lugo et al., 1999), have been used to map regions or even the entire globe. These maps have been created using observational (Kottek et al., 2006) as well as climate model data, the latter including CMIP5 ~~(Rahimi et al., 2020)~~ (Rahimi et al., 2020; Phillips and Bonfils, 2015) and CMIP6 climate models (Kim and Bae, 2021). Despite the changes and updates suggested by various authors, the classification scheme as originally developed by Köppen, and updated by Geiger is still ~~the most~~ a highly popular climate classification system. ~~The KG system has been applied to a broad spectrum of scientific interests, including to locally adjust an irradiation model (Every et al., 2020), in hydrological studies (Peel et al., 2001), and in modelling the distribution of Lyme disease (Cox et al., 2021).~~ Although bioclimate maps for specific years (such as 2100) have previously been created (Beck et al., 2018), an area that is less explored are global KG climate maps at specific levels of global warming. To remove the leading order uncertainty that arises from different climate model sensitivities to radiative forcing (Sherwood et al., 2020; Nijsse et al., 2020), and to make our results

relevant to the Paris climate targets (Paris-Agreement), here we look at changes in KG classification at different levels of global warming (1.5K, 2K, and 4K). A streamlined KG scheme is also implemented to visually demonstrate the impacts of warming on global biome distribution.

~~Here we present KG classification~~ KG classification maps at 1.5K, 2K, and 4K of global warming above reference period levels (taken as the 1901 – 1931 global mean temperature) are presented. Due to the 30 different classifications in the traditional KG scheme, it can be difficult to identify the changes in bioclimate classification ~~, so~~ we present a novel "streamlined" classification system that allows for easy identification of bioclimate change, with a naming scheme that is more intuitive. To ~~enhance~~ quantify this, classification change matrices ~~have been produced to quantify the changes displayed in the maps.~~

~~Furthermore, we utilise the KG system as an exploratory technique for understanding CMIP6 model output, the KG classification scheme has been previously applied to CMIP5 data to to evaluate simulations (Phillips and Bonfils, 2015).~~ are also given. By comparing the classifications given by models under the historical experimental run to the known historical observational values, and by assessing model deviation from their initial classifications, we gain insight into the performance and behaviours of individual models as well as ~~their~~ the multi-model ensemble mean.

We show there are large shifts in bioclimate distribution under global warming, with an almost exclusive change from colder, wetter bioclimates to hotter, dryer ones. Specifically we find the fraction ($f$) of the land experiencing a change in its bioclimatic class has a weakly-saturating dependence on global warming $f = 1 - e^{-0.14\Delta T}$, which implies about 13% of land experiencing a major change in climate, per 1K increase in global mean temperature between the global warming levels of 1 and 3K.

## 2  Methods

### 2.1  Köppen-Geiger classification scheme

The Köppen-Geiger (KG) classification scheme has been described extensively in other publications (Peel et al., 2007; Beck et al., 2018). The scheme has also undergone many alterations. Here we follow (Peel et al., 2007), whose criteria for each classification are given in Table 1.

These classifications have three differences to those described by (Köppen, 1936). First, C and D climates follow a 0˚C threshold instead of ~~3~~ 3˚C (Russell, 1931). Secondly, BW and BS are distinguished using a 70% threshold for precipitation seasonality (Peel et al., 2007). Finally, climates C and D subclassifications s and w are made mutually exclusive (Peel et al., 2007) . In this analysis, each month is set to have the same length of time – one twelfth of a year.

The KG system has been applied to a broad spectrum of scientific interests, including to locally adjust an irradiation model (Every et al., 2020), in hydrological studies (Peel et al., 2001), and in modelling the distribution of Lyme disease (Cox et al., 2021) .

### 2.1.1  Streamlined Köppen-Geiger classification scheme

| Classification | | | Criteria | Classification | | | Criteria |
|---|---|---|---|---|---|---|---|
| A | | | Tmin ≥ 18°C | D | | | Tmin $<$ 0°C, Tmax ≥ 10°C |
| | F | | Pmin ≥ 6 cm month$^{-1}$ | | W | | Pswet $>$ 10*Pwdry |
| | S | | Pmin ≥ 100-(Pyear*10/25) | | S | | 3*Psdry <Pwwet, Psdry < 4 |
| | W | | Pmin <100-(Pyear*10/25) | | F | | Neither W nor S |
| B | | | Pyear*10 <10*Pthresh | | | a | Tmax ≥ 22°C, Months above 10°C ≥ 4 |
| | W | | Pyear*10 <5*Pthresh | | | b | Tmax <22°C, Months above 10°C ≥ 4 |
| | S | | Pyear*10 ≥ 5*Pthresh | | | c | 0 <Months above 10°C <4, not A or B or D |
| | | h | Tavg ≥ 18°C | | | d | Tmin <-38°C, 0 <Months above 10°C <4 |
| | | k | Tavg <18°C | E | | | Tmax <10°C |
| C | | | 0°C $<$ Tmin <18°C, Tmax ≥ 10°C | | T | | 0°C $<$ Tmax <10°C |
| | W | | Pwdry <Pswet/10 | | F | | 0°C ≥ Tmax |
| | S | | Pwwet $>$ 3*Psdry, Psdry <4 | | | | |
| | F | | Neither W nor S | | | | |
| | | a | Tmax ≥ 22°C, Months above 10°C ≥ 4 | | | | |
| | | b | Tmax <22°C, Months above 10°C ≥ 4 | | | | |
| | | c | 0 <Months above 10°C <4, not A or B | | | | |

**Table 1.** Classification criteria for the Köppen-Geiger classification scheme. Tmin = Average temperature of month with lowest average temperature. Tmax = Average temperature of month with highest average temperature. Pmin = Average precipitation of driest month. Pmax = Average precipitation of wettest month. Tavg = Mean annual temperature. Pyear = Mean annual precipitation. Pthresh varies according to the following rules (if 70% of Pyear occurs in winter then Pthresh = 2 x Tavg, if 70% of Pyear occurs in summer then Pthresh = 2 x Tavg + 28, otherwise Pthresh = 2 x Tavg + 14). , Psdry = precipitation of the driest month in summer, Pwdry = precipitation of the driest month in winter, Pswet = precipitation of the wettest month in summer, Pwwet = precipitation of the wettest month in winter. In the northern Hemisphere Summer is defined as AMJJAS and Winter as ONDJFM, the opposite is true for the Southern hemisphere. Due to overlapping criteria, dry (B) climates are prioritised above all others. Temperature is in °C and precipitation is cm month$^{-1}$ and cm year$^{-1}$. Here we follow (Peel et al., 2007).

A key goal of bioclimatic classifications is to illustrate climate change in a way that is intuitive. To this end we designed a simplified Köppen-Geiger scheme which combines classifications to make changes clearer in both scale and the nature of projected transitions. Additionally, the new scheme implements a more traditional naming system. A breakdown of this streamlined system, and the constituent traditional classifications involved in each of the thirteen streamlined classifications is given in Table 2.

Difference maps are also plotted to demonstrate the geographical locations of major transitions between bioclimatic classifications. These difference maps plot the ten largest transitions globally (by total land area).

| Streamlined Classification | Traditional Classifications |
| --- | --- |
| Desert | BWh, BWk |
| Semi-Arid | BSh, BSk |
| Tropical Rainforest | AF |
| Tropical Monsoon | AM |
| Tropical Savanna | AW |
| Mediterranean | CSa, CSb, CSc |
| Subtropical | CWa, CWb, CWc, CFa |
| Oceanic | CFb, CFc |
| Continental hot-summer | DFa, DSa, DWa |
| Continental cold-summer | DFb, DSb, DWb |
| Sub Arctic | DFc, DFd, DSc, DSd, DWc, DWd |
| Arctic Tundra | ET |
| Icecap | EF |

**Table 2.** Breakdown of the streamlined classification scheme and the assignment of traditional classifications within the new scheme.

Classification change matrices are used to quantify bioclimate transitions in terms of global land area, at key levels of global warming. The columns represent the initial classification coverage, and the rows indicate the altered classification distribution. Shading highlights the size of changes, in terms of the projected change as a fraction of the initial area of a given bioclimatic class.

## 2.2 Climate Model and Observational Data

Historical observations of monthly mean temperature and precipitation are from the CRU TS v. 4.05 dataset (Harris et al., 2020). Analogous climate model data comes from the 'historical' CMIP6 experiments (Eyring et al., 2016). ~~Six models~~ Models within the CMIP6 multi-model ensemble were chosen ~~for reasons of datamanagement, these being CanESM5~~ which had readily available historical experiment data, and achieved a minimum of 4K warming under the ssp585 scenario. These models are listed in Table 4.

CMIP6 model data ~~is~~ was regridded to 0.5˚ by 0.5˚, the same spatial resolution as CRU TS observations. Antarctica ~~is~~ was excluded as observations are limited in this region, and ~~no significant~~ we do not expect substantial changes in bioclimatic classification ~~are expected~~ in this region.

The model output data is typically at a coarser resolution than the underlying 0.5˚ climatology. The anomaly corrected fields therefore contain spatial variability that is solely due to the underlying climatology at scales which are not resolved by a model.

| Model | Institution | Frequency | Nominal Resolution | Publication |
|---|---|---|---|---|
| CanESM5 | CCCma | mon | 100 km | (Swart et al., 2019d) (Swart et al., 2019a) |
| CanESM5-CanOE , | CCCma | mon | 100 km | (Swart et al., 2019c) (Swart et al., 2019b) |
| CESM2 , | NCAR | mon | 100 km | (Danabasoglu, 2019b) (Danabasoglu, 2019a) |
| CESM2-WACCM , | NCAR | mon | 100 km | (Danabasoglu, 2019c) (Danabasoglu, 2019d) |
| IPSL-CM6A-LR and | IPSL | mon | 100 km | (Boucher et al., 2018) (Boucher et al., 2019) |
| UKESM1-0-LL . | Met Office Hadley Centre | mon | 100 km | (Tang et al., 2019) (Good et al., 2019) |
| ACCESS-CM2 | CSIRO-ARCCSS | mon | 250 km | (Dix et al., 2019b) (Dix et al., 2019a) |
| AWI-CM-1-1-MR | NCAR | mon | 100 km | (Danek et al., 2020) (Semmler et al., 2019) |
| CAS-ESM2-0 | UCI | mon | 100 km | (Chai, 2020) (Cas, 2018) |
| EC-Earth3 | EC-Earth-Consortium | mon | 100 km | (EC-Earth-Consortium, 2019b) (EC-Earth-Consortium, 2019a) |
| EC-Earth3-Veg | EC-Earth-Consortium | mon | 100 km | (EC-Earth-Consortium, 2019d) (EC-Earth-Consortium, 2019c) |
| TaiESM1 | AS-RCEC | mon | 100 km | (Lee and Liang, 2020b) (Lee and Liang, 2020a) |

**Table 3.** Details of the models used in this study.


This also implies that the diagnosed changes in bioclimatic types (which are dependent on the model anomalies) tend to be somewhat smoother at these finer spatial scales.

## 2.3 Model performance assessment

Comparison of KG observed classifications with the CMIP6 models simulated classifications is made for the years 1901-2014.
115 To reduce the effect of short-term variability model and observational data is are smoothed with a 30 year centred rolling mean.

The ability of individual models in the CMIP6 ensemble to simulate KG classifications correctly of observational data during the historical period is assessed in two ways: (i) Percentage land area that a model has correctly classified for each year

relative to observations. (ii) Percentage change in land area classification at each year compared to the initial mean 1901-1931 classifications.

## 2.4 ~~Warming~~ Maps of KG classification versus global warming

Future KG classification maps under 1.5, 2 and 4K of annual mean global warming above ~~pre-industrial~~ reference period levels were created from the CMIP6 ~~model~~ 'ssp585' 2015-2100 future scenario. We used ssp585 because all models pass 4K under ssp585, which enables us to define changes in bioclimatic zones consistently for these different levels of global warming.

The timing of each warming level is found from the centred 30 year annual mean global surface air temperature above the model's reference temperature, here defined as 1901 – 1931. Monthly mean anomalies of precipitation and surface air temperature are calculated relative to this same reference period. ~~Where anomaly corrected fields of precipitation and temperature are used, these are calculated as the sum of the mean observations (~~Model outputs are anomaly corrected to agree with the observational over the period 1901-1931~~) and an individual model's anomalies at the specified warming level. Ensemble~~. This is done by calculating anomalies relative to that period for each model and then adding these anomalies to the observational climatology. Multi-model ensemble mean KG classification maps are calculated using the multi-model ensemble mean of the anomalous temperature and precipitation fields at each warming level.

### 2.4.1 ~~Streamlined Köppen-Geiger classification scheme~~

~~A key goal of bioclimatic classifications is to illustrate climate change in a way that is more intuitive for many people. To this end we designed a simplified Köppen-Geiger scheme which combines classifications to make changes clearer in both scale and the nature of projected transitions. Additionally, the new scheme implements a more traditional naming system. A breakdown of this streamlined system, and the constituent traditional classifications involved in each of the thirteen streamlined classifications is given in Table 2.~~

~~**Streamlined Classification Traditional Classifications** Desert BWh, BWk Semi-Arid BSh, BSk Tropical Rainforest AF Tropical Monsoon AM Tropical Savanna AW Mediterranean CSa, CSb, CSc Subtropical Cwa, CWb, CWc, Cfa Oceanic CFb, CFc Continental hot-summer Dfa, Dsa, Dwa Continental cold-summer DFb, DSb, DWb Sub Arctic DFc, DFd, DSc, DSd, DWc, DWd Arctic Tundra ET Icecap EF Breakdown of the streamlined classification scheme and the assignment of traditional classifications within the new scheme.~~

~~Difference maps are also plotted to demonstrate the geographical locations of major transitions between bioclimatic classifications. These difference maps plot the ten most significant transitions globally (by total land area).~~

~~Classification change matrices are used to quantify bioclimate transitions in terms of global land area, at key levels of global warming. The columns represent the initial classification coverage, and the rows indicate the altered classification distribution. Shading highlights the significance of changes, in terms of the projected change as a fraction of the initial area of a given bioclimatic class.~~

# 3   Results and discussion

## 3.1   Model performance assessment

To gain insight into the behaviour of individual models, we create KG maps of individual models and compare ~~them~~ these
with maps derived from the observed climate. As expected, there is variation in the classification distribution of models and
the observational data. For example, desertification in the Amazon is apparent in CanESM5 and CanESM5-CanOE models
(Appendix A). This may show that these models have a tendency towards reduced precipitation in the tropics when compared
to other models. Another area of disagreement between the models is the change of biome classification in northern Eurasia
and America at various levels of global warming. The multi-model ensemble mean model state however reduces the effect of
individual model discrepancies and compares favourably with observations.
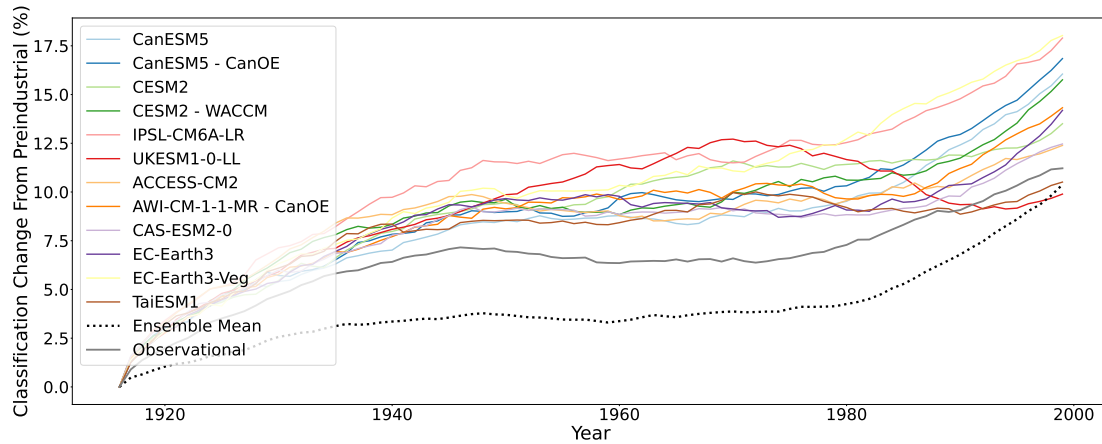
**Figure 1.** The percentage land area change ~~from~~ in K-G classification for each model versus year through the ~~initial 1916 classifications~~ 20th century (without anomaly correction). ~~Showing~~ The equivalent trajectory based on the ~~ensemble mean with reduced classification area change compared to models and the observational due to model variation minimisation~~ observed climate is shown for comparison in ~~the meaning process~~ dark-grey. ~~Strong agreement between models and~~ The dotted line shows the ~~observational~~ trajectory derived from the ensemble mean climate.
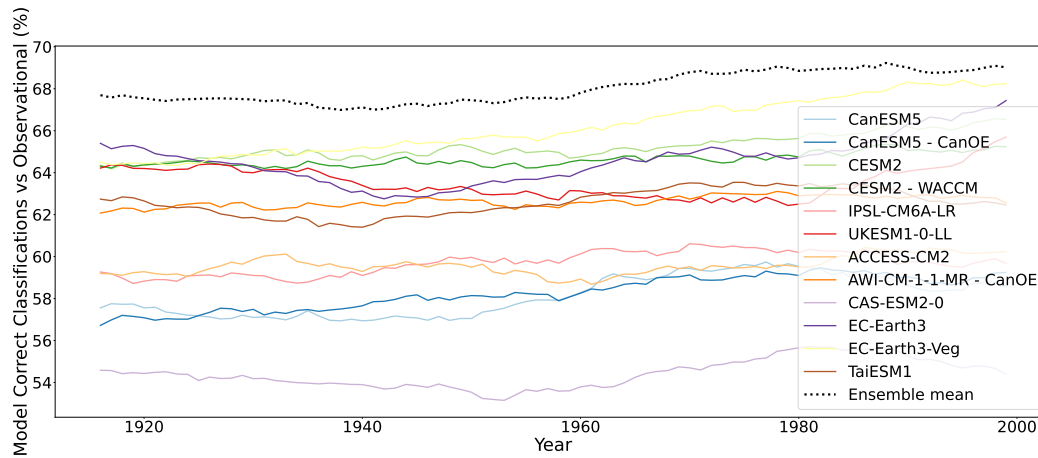


**Figure 2.** The percentage land area correctly classified (without anomaly correction). ~~Showing the ensemble mean as the most consistently correctly classified area compared to the observational due to model variation minimisation in the meaning process. Shows the models initial states separate into two groups.~~

In Figure ~~1.~~ 1 simulated classification changes from the CMIP6 historical runs are compared to those calculated from the observed climate. The CMIP6 models broadly capture the degree of expected global classification change. All models show a

160 similar behaviour – a ~~significant~~ large change in classifications at the start of the observed period until 1940, the mid-century then presents an approximately constant set of classification with very little change until 1980, where again all models display further changes in climate classification. Although the multi-model ensemble mean follows the same pattern as the individual models and the observational data, it shows a lesser degree of change throughout the observed time period. This reduced variation is inherent to the nature of this ensemble mean; large changes in individual models have their impact reduced in the

165 meaning process. This may lead to the ~~ensemble mean~~ multi-model ensemble mean displaying a similar but mitigated and delayed trend 'lagging' the individual models and the observational when creating discrete classes from climate data.

To assess the performance of individual models and their multi-model ensemble mean in ~~correctly~~ classifying the bioclimate distribution according to observation-based KG for a particular year, the percentage land area correctly classified by each model every year according to observation-based KG is shown in Figure 2. The results show that the ensemble mean is one of the best

170 performing for classification. This is in contrast to Figure 1 which showed the ensemble mean was one of the worst performing for classification change. The reason is also likely due to the reduced variation in data resulting from the averaging process in the creation of the multi-model ensemble mean dataset. The impact of 'extreme' values present in each model are averaged out in the multi-model ensemble mean provided they are distributed around the 'true' climate values. This would suggest that for individual time points, the ensemble mean is likely to provide the the most reliable projection. The results from Figure 1 and

175 Figure 2 give insight into the behaviour of ensemble mean datasets and when their application is appropriate. Traditionally the ensemble mean has been taken as the most likely scenario and therefore the most representative of the real-world climate. The results presented here indicate that although the ensemble mean is appropriate for assessing model output at individual points, the ensemble mean does not accurately display the variability evident in ~~real world~~ observed climate data.

### 3.2 ~~Warming maps~~ Maps of KG classification versus global warming

180 Figure 3 shows the multi-model ensemble model mean KG classification for 1.5K, 2K and 4K of global warming above the reference period, as well as the no warming classifications. Plots for individual models for the reference period without anomaly correction, and at 1K, 1.5K, 2K, 3K, and 4K of global warming with anomaly correction, are shown in ~~the appendix~~ appendix A under the traditional scheme, and Appendix B under the streamlined scheme. Comparison to the reference climate ~~shows that there will be a~~ suggests that there could be dramatic changes in bioclimate classification, particularly in the mid-

185 to high latitudes, as the planet warms. These changes become more apparent in Figure 4, which use the streamlined KG classification scheme and ~~are chosen to highlight the ten most significant~~ highlights the ten largest bioclimatic shifts for each level of warming.
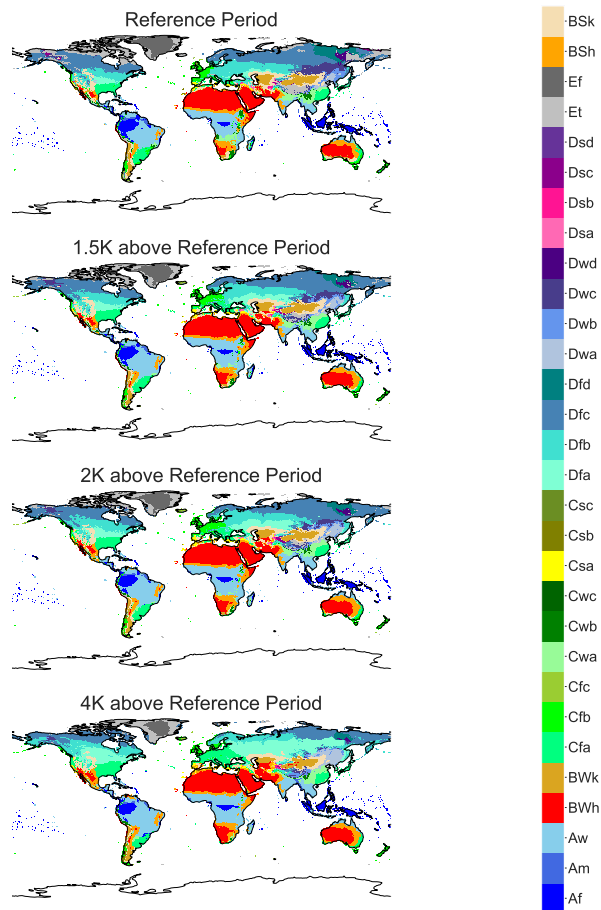
**Figure 3.** ~~Anomaly plot~~ Maps of the original K-G classifications calculated from the multi-model ensemble mean ~~CMIP6 ssp585 runs~~ for the reference period ~~,~~ and 1.5K, ~~2K~~2.0K, ~~and 4K~~ 4.0K of global warming ~~with~~ relative to the ~~traditional Köppen-Geiger classification system applied~~reference period. ~~Note~~ These were calculated from the ~~large changes in northern America and Eurasia~~SSP585 runs by anomaly correcting relative to the observed reference climate .
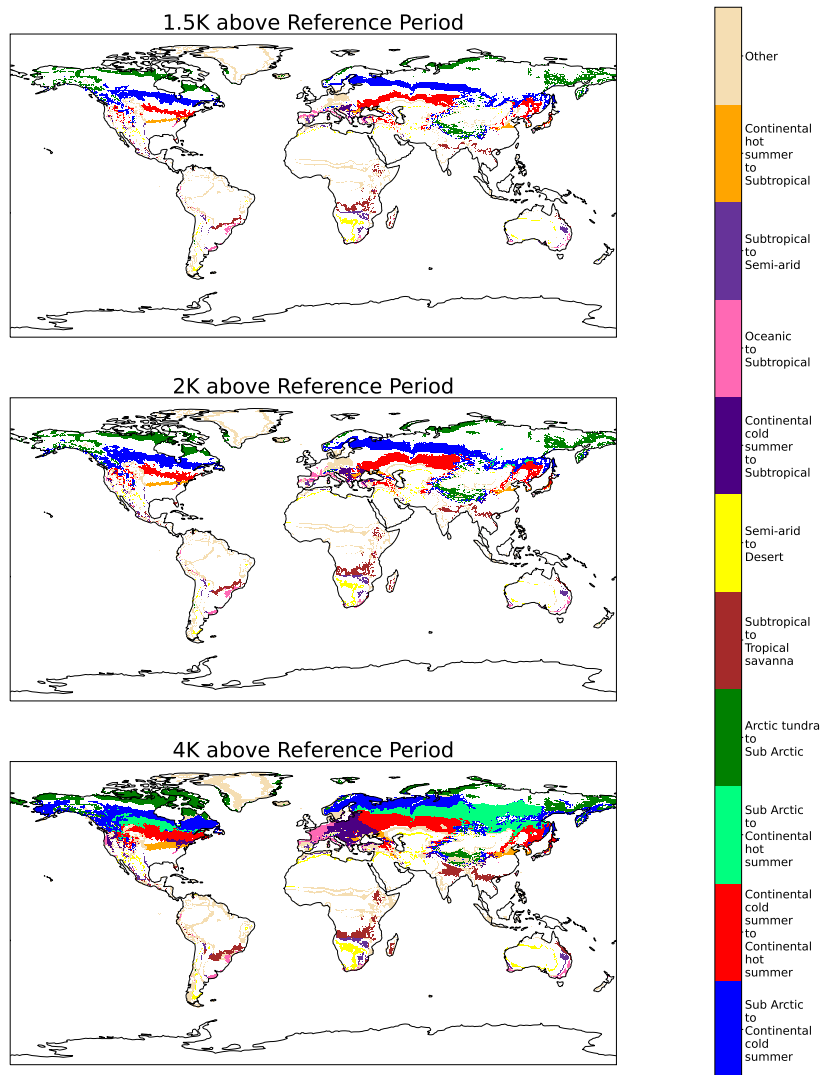
**Figure 4.** ~~Ensemble~~ Multi-model ensemble mean difference maps highlighting the ten largest classification changes for 4K of warming above the reference period using the streamlined classification system.
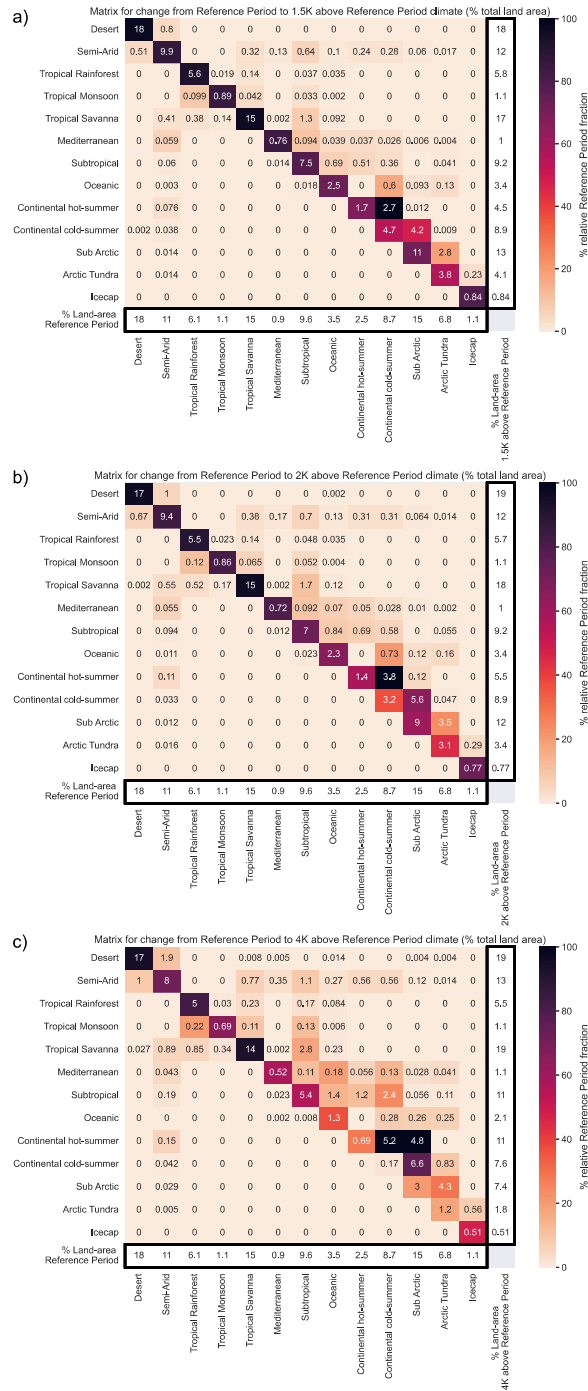
**Figure 5.** ~~Ensemble~~ Multi-model ensemble mean difference matrices highlighting the classification changes for levels of warming above the reference period of a) 1.5K, b) 2K, c) 4K, using the streamlined classification system.

These shifts are almost exclusively from wetter and colder classes to drier and hotter ones as the global temperature increases. This agrees strongly with the results found by Feng et al. (2014), which under CMIP5's RCP8.5 scenario, suggested bioclimatic

190 shifts toward warmer and drier types across the global region with climate change. Large areas undergo desertification in the southern hemisphere. The majority of North America and Northern Eurasia has a shift towards warmer climates as Sub-arctic gives way to continental cold summer, and continental cold summer is replaced by continental warm summer. All changes in classification with the streamlined KG scheme are quantified in Figure 5.

At 4K ~~these~~ areas of classification change represent over ~~15~~33% of land area. The change in % of total land-area in Figure ~~5a~~

195 5c gives some alarming perspectives, for example, at +4K Arctic Tundra is indicated to cover over ~~40%~~ a quarter less land-area than in in the reference period. At 2K the models already project ~~significant~~ substantial changes to the global distribution of bioclimates; at 4K these changes become even more pronounced.

| Classification | Change in global land area coverage (%) per degree of warming ($K$) | Coefficient of determination ($r^2$) |
|---|---|---|
| Desert | $0.30 \, \% K^{-1}$ | 0.93 |
| Semi Arid | $0.35 \, \% K^{-1}$ | 0.94 |
| Tropical Rainforest | $-0.26 \, \% K^{-1}$ | 0.96 |
| Tropical Monsoon | $0.09 \, \% K^{-1}$ | 0.97 |
| Tropical Savanna | $1.01 \, \% K^{-1}$ | 0.97 |
| Mediterranean | $0.07 \, \% K^{-1}$ | 0.33 |
| Subtropical | $0.25 \, \% K^{-1}$ | 0.20 |
| Oceanic | $-0.35 \, \% K^{-1}$ | 0.94 |
| Continental Hot-Summer | $2.18 \, \% K^{-1}$ | 0.98 |
| Continental Cold-Summer | $-0.25 \, \% K^{-1}$ | 0.21 |
| Sub Arctic | $-2.03 \, \% K^{-1}$ | 0.97 |
| Arctic Tundra | $-1.24 \, \% K^{-1}$ | 0.95 |
| Icecap | $-0.13 \, \% K^{-1}$ | 0.99 |
| Streamlined Total Change | $10.85 \, \% K^{-1}$ | 0.99 |
| Traditional Total Change | $11.91 \, \% K^{-1}$ | 0.97 |

**Table 4.** Percentage change in the global land area of each of the streamlined classifications per degree of global warming. Change is based on linear approximations of results from reference period to 4K of warming

In Table 4 we give the percentage change in global land area of each of the streamlined classifications per degree of warming assuming the dependence is linear up to 4K of warming. Linear dependence is a good approximation for most classifications

200 with all but three having $r^2 > 0.9$. The three poorly fitting classifications, those for Mediterranean, subtropical, and continental cold-summer bioclimates, may be transitory classifications whose peak or minimum land area coverage is within the 4K range the linear equation is based on. Classifications predicted to decrease in global fraction under global warming (with good $r^2$) are tropical rainforest, oceanic, sub Arctic, Arctic tundra and icecap, the largest decrease of which globally is sub Arctic

**14**

(2.03 %$K^{-1}$). Classifications that increase under global warming with good certainty are desert, semi arid, tropical monsoon, tropical savanna and continental hot-summer with the largest increase predicted to be continental hot-summer (2.18 %$K^{-1}$). Raw plots for these fits without lines fitted can be found in Appendix C2.

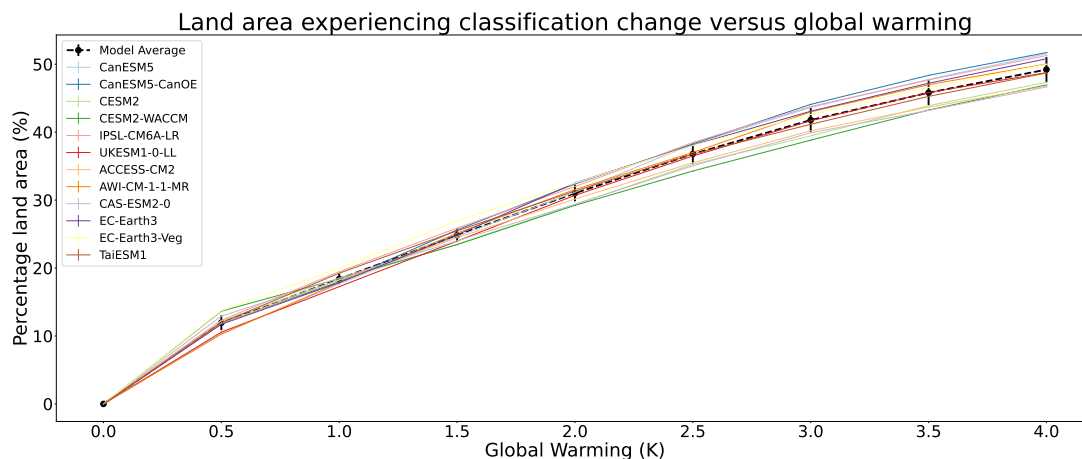### 3.3 Sensitivity of bioclimate to global warming



**Figure 6.** The percentage of land area projected to see a change in bioclimate as a function of global warming, using the traditional Köppen-Geiger classification with anomaly correction. Note the robust agreement between models, which implies ~~an~~ a multi-model ensemble mean change which is well approximated by: $f = 1 - e^{-0.17\Delta T - 0.14\Delta T}$.

Figure 6 displays a weakly-saturating increase with global warming, the fraction of land area that experiences a change in classification follows Eq. (1):

$$f = 1 - e^{-k\Delta T} \tag{1}$$

where $f$ is the fraction of land area that experiences a change in bioclimatic classification, $\Delta T$ is the global warming relative to the reference period climate, and $k$ is a fitting parameter. The mean response across the models suggests a value of ~~$k \sim 0.17$~~ $k \sim 0.14$ $K^{-1}$. This was calculated to have a coefficient of determination of 0.84. For the range of global warming of particular interest to the Paris climate agreement (1 to 3 degrees of warming) the land area experiencing a change in bioclimatic classification is approximately ~~12~~13% of the global land per Kelvin of global warming. The total land area (neglecting Antarctica) is approximately 146 million square kilometres, so this implies a bioclimatic change for ~~over 17.5~~ 18.9 million square kilometres of land per degree of warming between 1K and 3K. This highlights the benefits of keeping global warming to 1.5K as opposed to 2K of warming, as the 0.5K difference represents an additional bioclimatic change for over ~~7~~7.5 million square kilometres of land. Previous studies of classification change with global warming have been regional, studies such as

220  Kim and Bae (2021) suggest a classification area change of approximately 15% of Asian monsoon regions at 2K of warming, regional assessments at the equator or in the southern hemisphere are likely to under represent global changes in classification however as the majority of classification change is predicted to be north of 30°N (Feng et al., 2014). A quantitative distribution of climate classification changes between global warming levels of 1.5K and 2K can be seen in Appendix b C (note that this breakdown uses the streamlined KG system and subsequently will not represent all changes included in Fig. Figure 6).

## 4 Conclusions

Despite the difference in climate projections for given greenhouse gas emissions, we present strong evidence that climate models agree well on the extent of bioclimatic change the global land-surface will undergo per degree of global warming. The Köppen-Geiger scheme has been used to present the impact of global warming at 1.5K, 2K, and 4K of warming above reference period levels in the form of climate maps – showing the global distribution of bioclimates, and as graphs and classification change matrices quantifying the degree of significant climate change for all classifications, at various levels of warming.

Despite the fact that these bioclimate Bioclimate classifications are fundamentally climate classifiers, but they are designed to represent and correlate with biome distribution. In this way the warming maps and classification changes represent tangible shifts in the global distribution of ecosystems, giving insight into the nature of Earth at various levels of warming. This paper also uses the Köppen-Geiger scheme as a method for climate model verification which is relevant to the impacts of climate change on ecosystems. The Köppen-Geiger maps at levels of global warming demonstrate the impact that climate change will could have. The transition matrices present an easily interpretable method for understanding and quantifying the scale of all classification changes. The results presented by the maps and matrices predict large changes in global bioclimate distribution, with hotter, drier bioclimates expanding and colder, wetter bioclimates shrinking and moving further towards the poles.

The combination of the techniques presented in this paper indicate that the impact of global warming on KG bioclimates is roughly linear for levels of warming between 1 and 3K. We find that 12 13% of land will experience a significant could experience a substantial change in bioclimate per $^o$C of global warming.
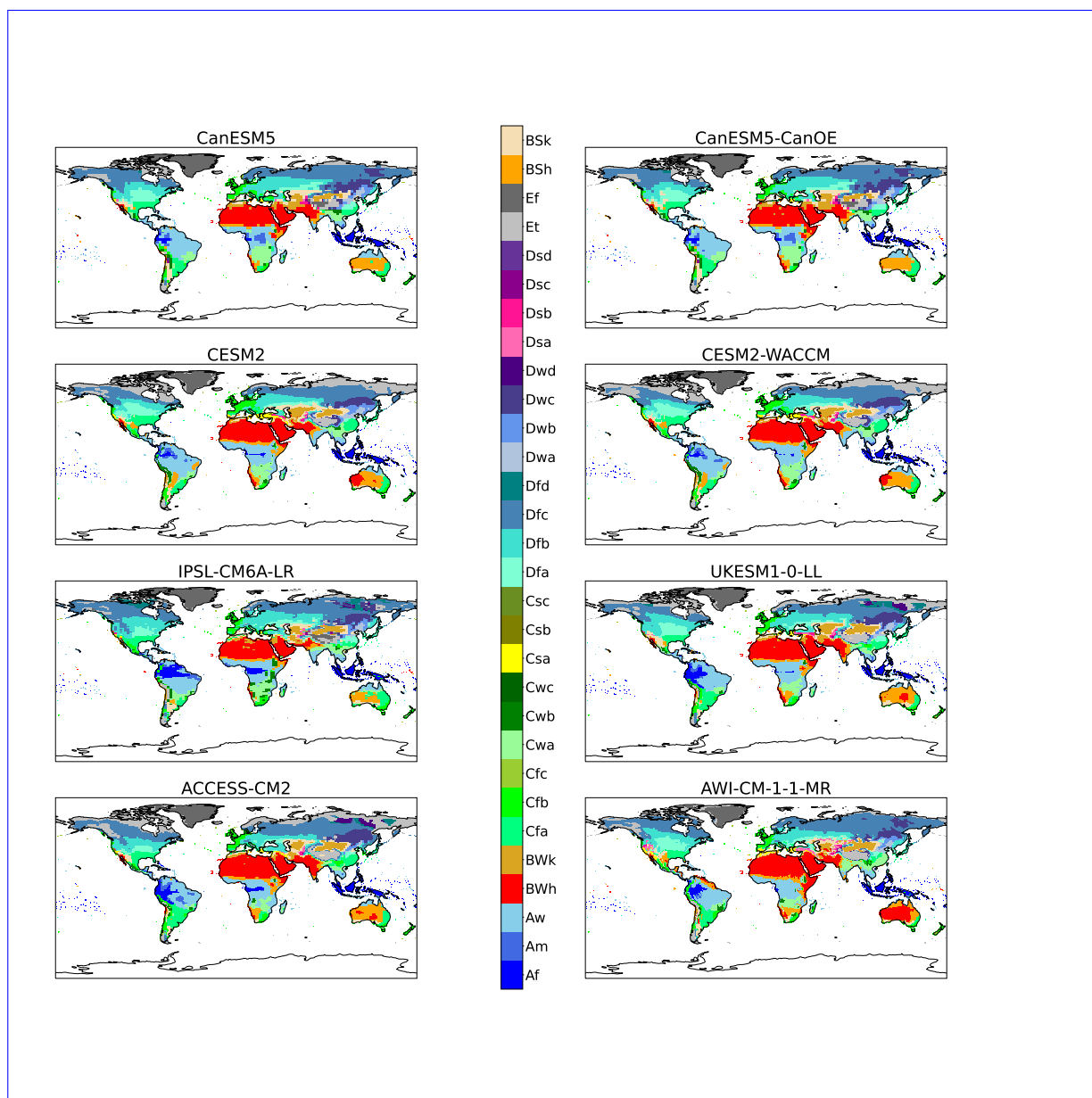
16

# Appendix A



**Figure A1.** ~~All models~~ Maps of KG classifications for each model for the reference period (1901 - 1931)~~(No~~, without anomaly correction~~)~~.
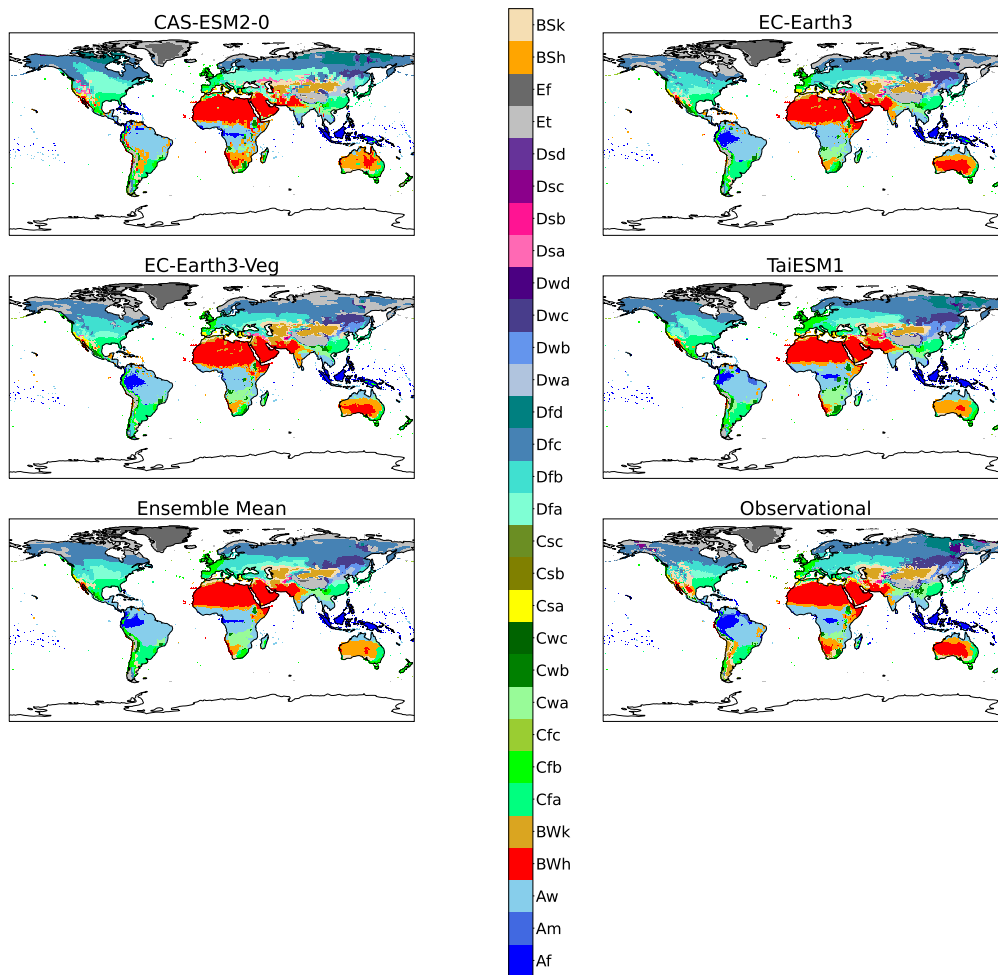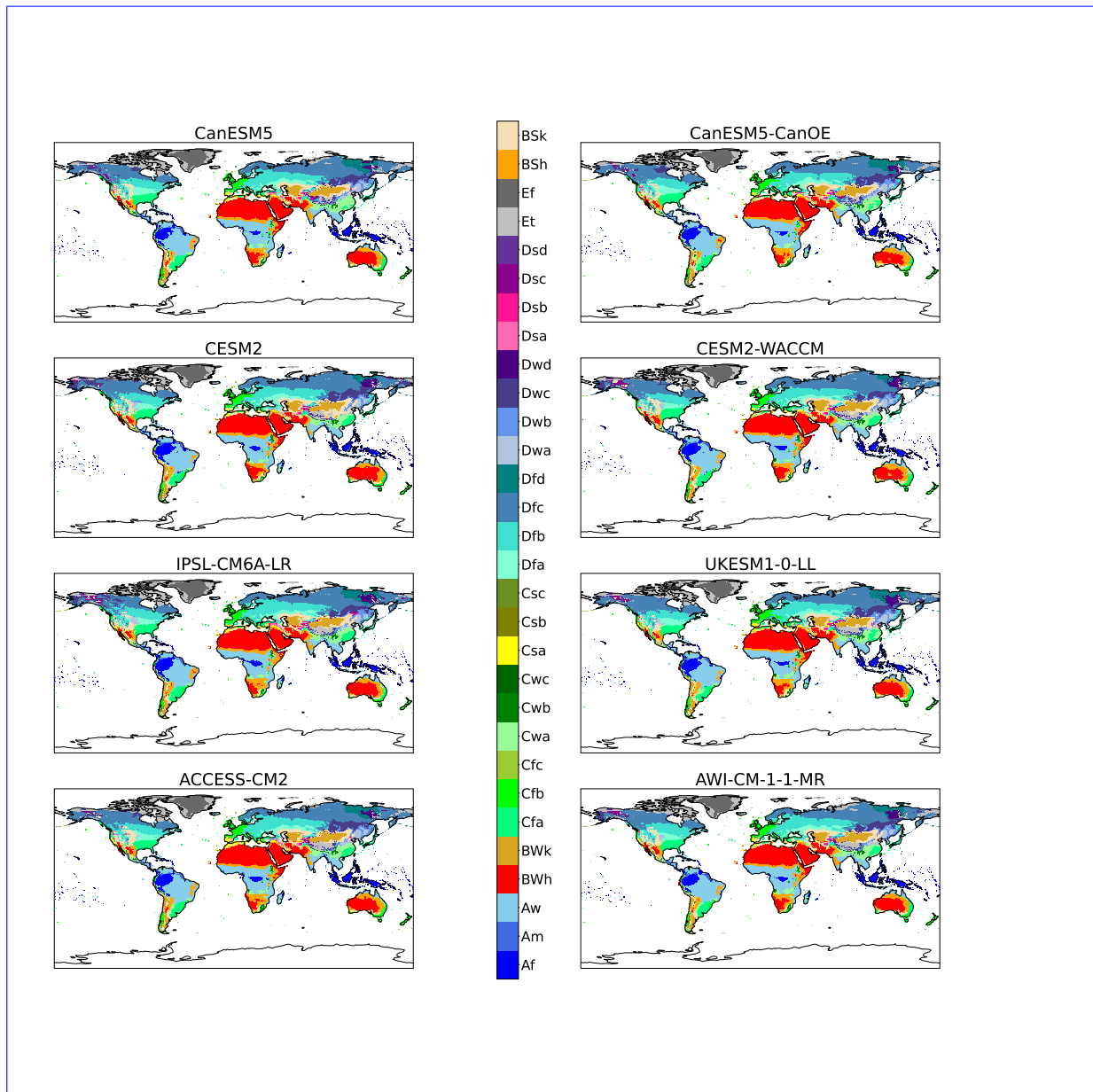
**Figure A1.** Continued.

**Figure A2.** ~~All models~~ Maps of KG classifications for each model at +1K, with anomaly correction.
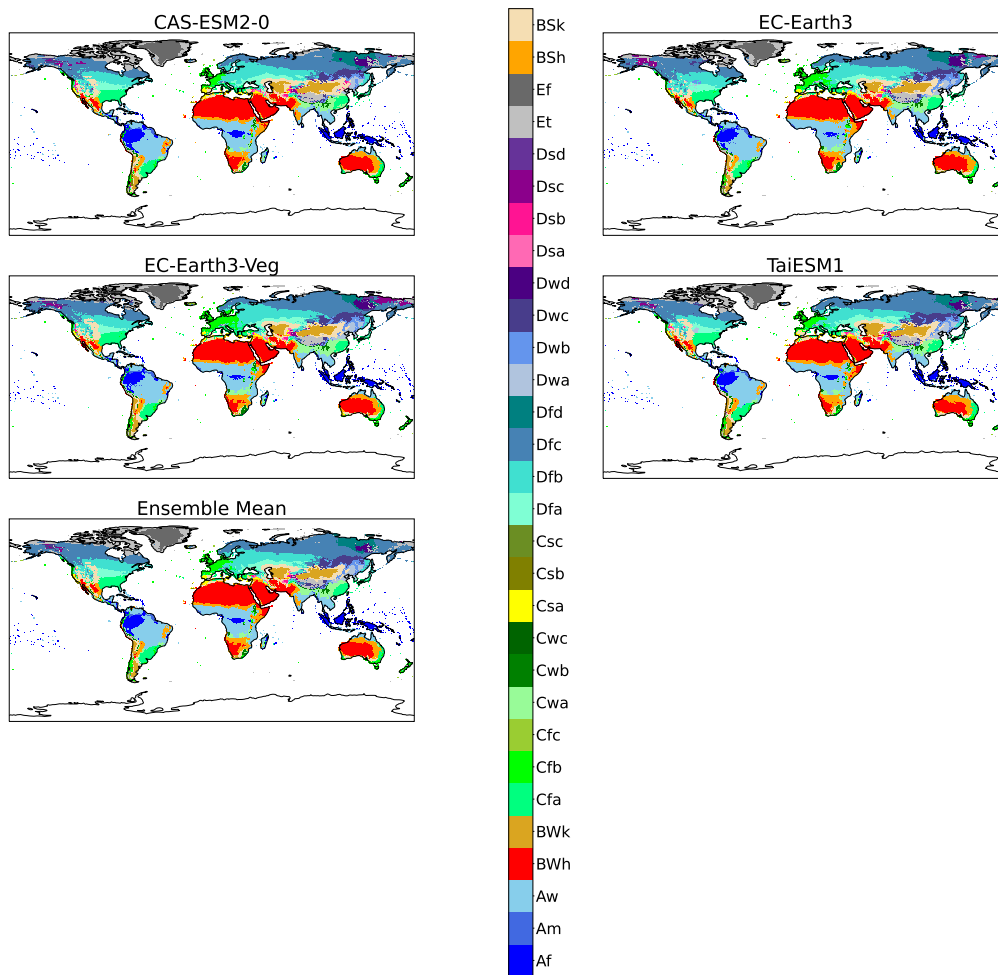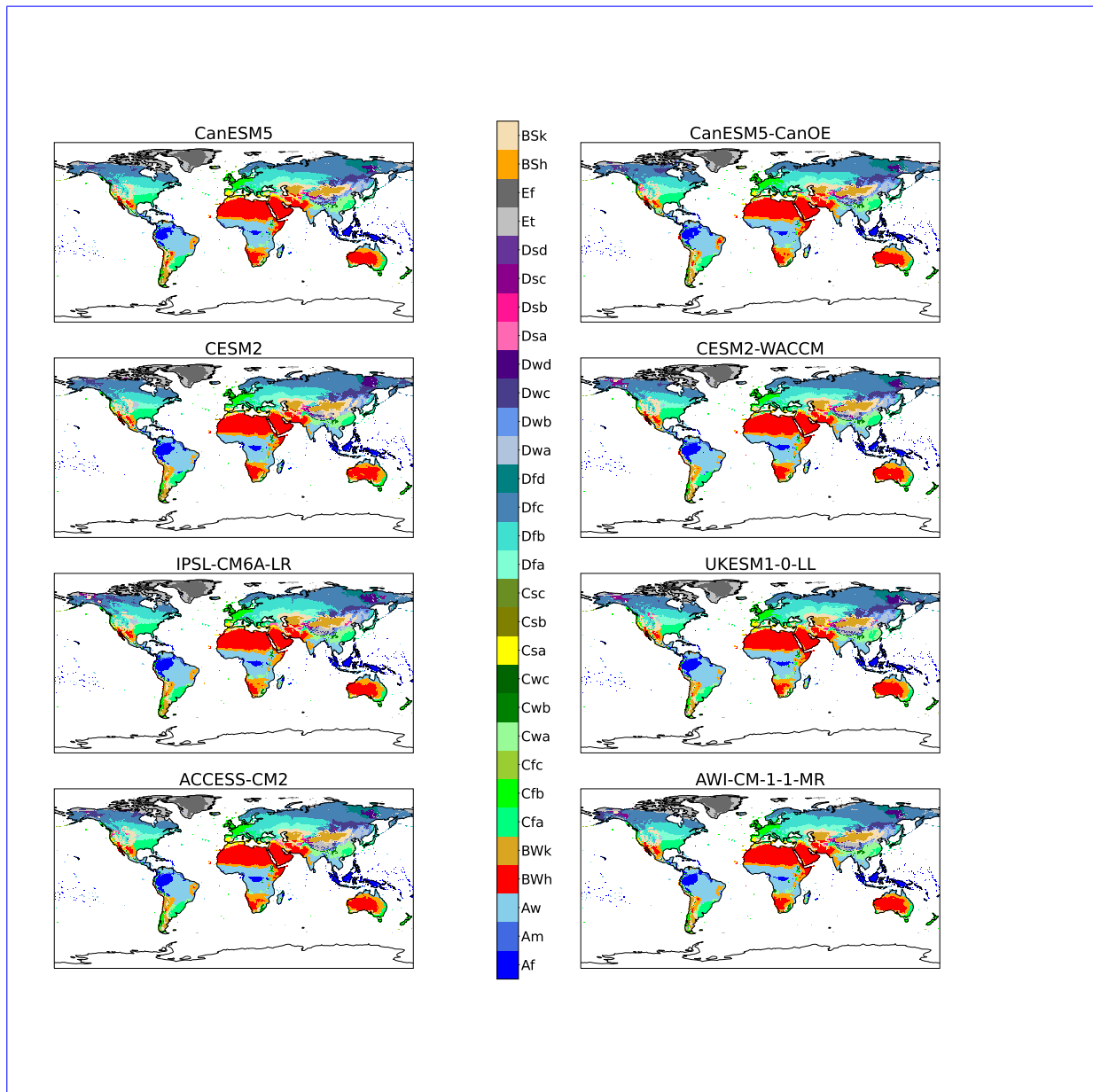
Figure A2. Continued.

**Figure A3.** Maps of KG classifications for each model at +1.5K, with anomaly correction.
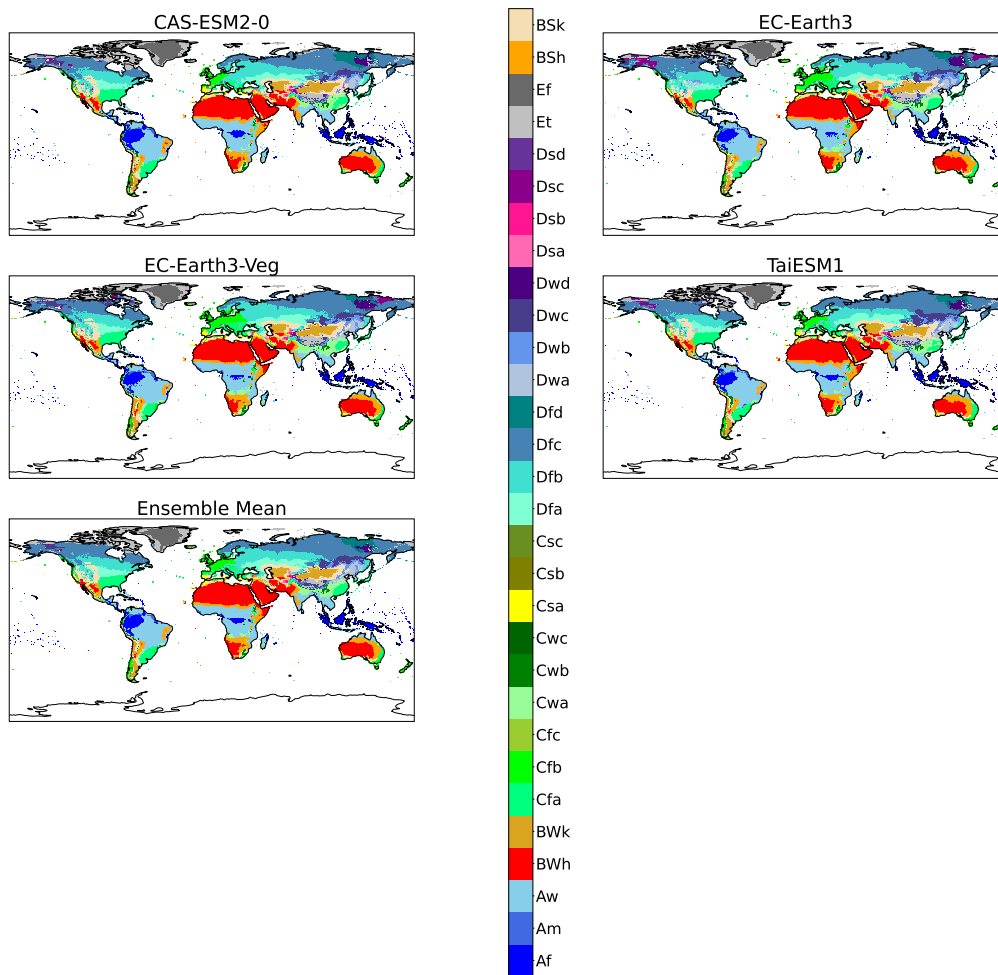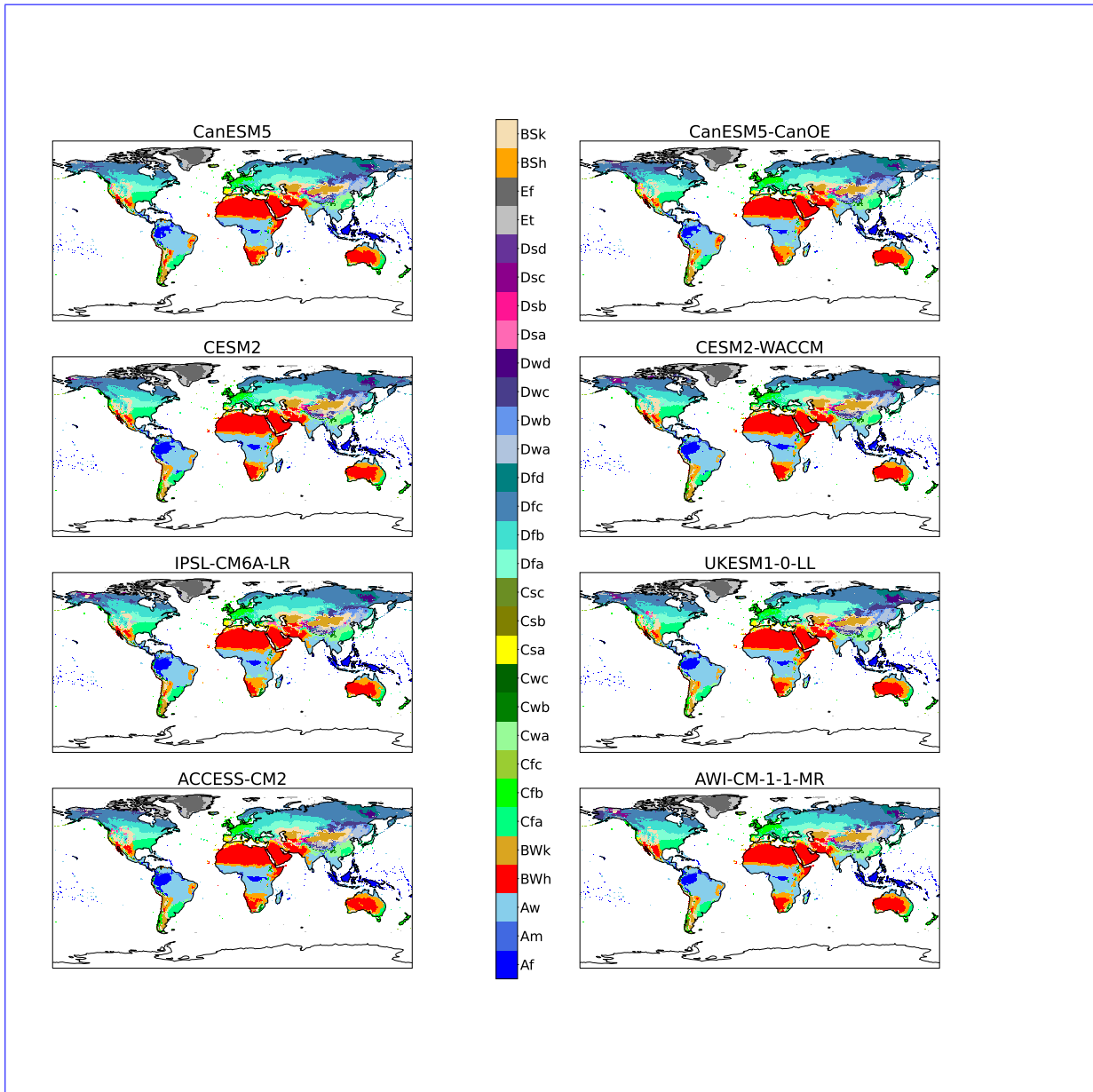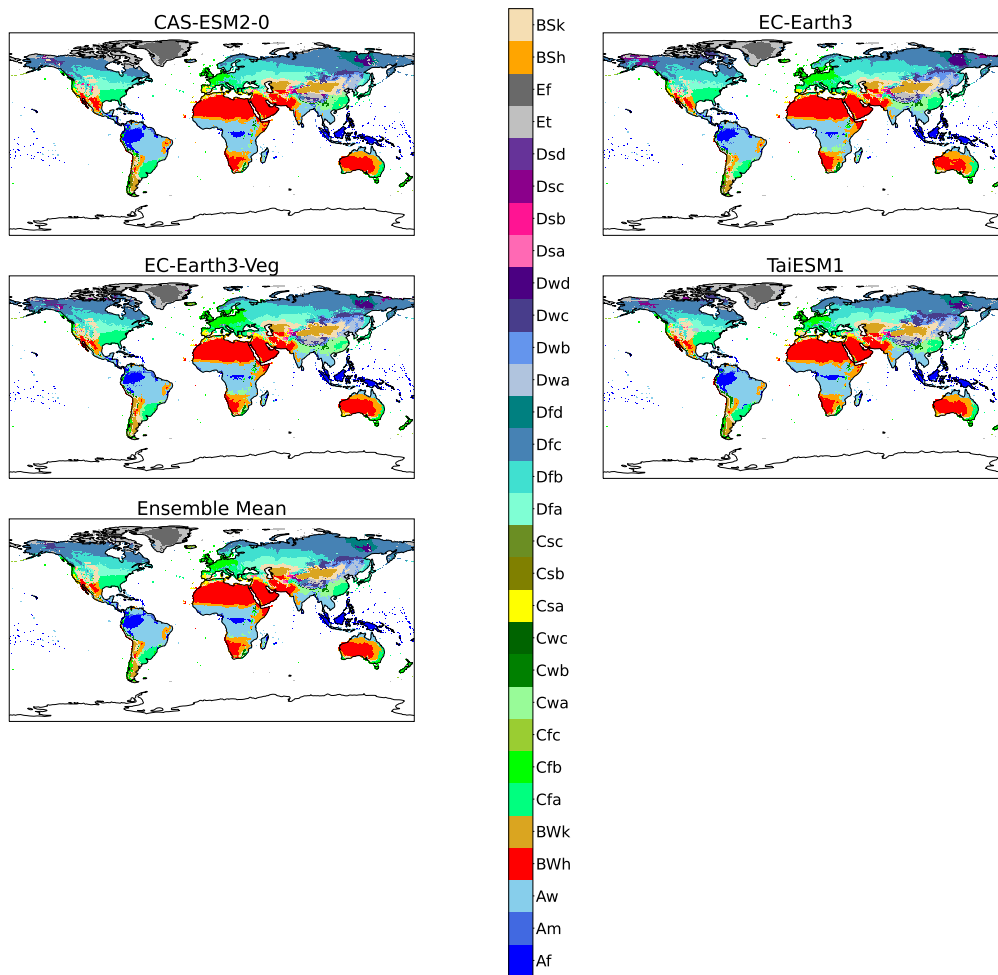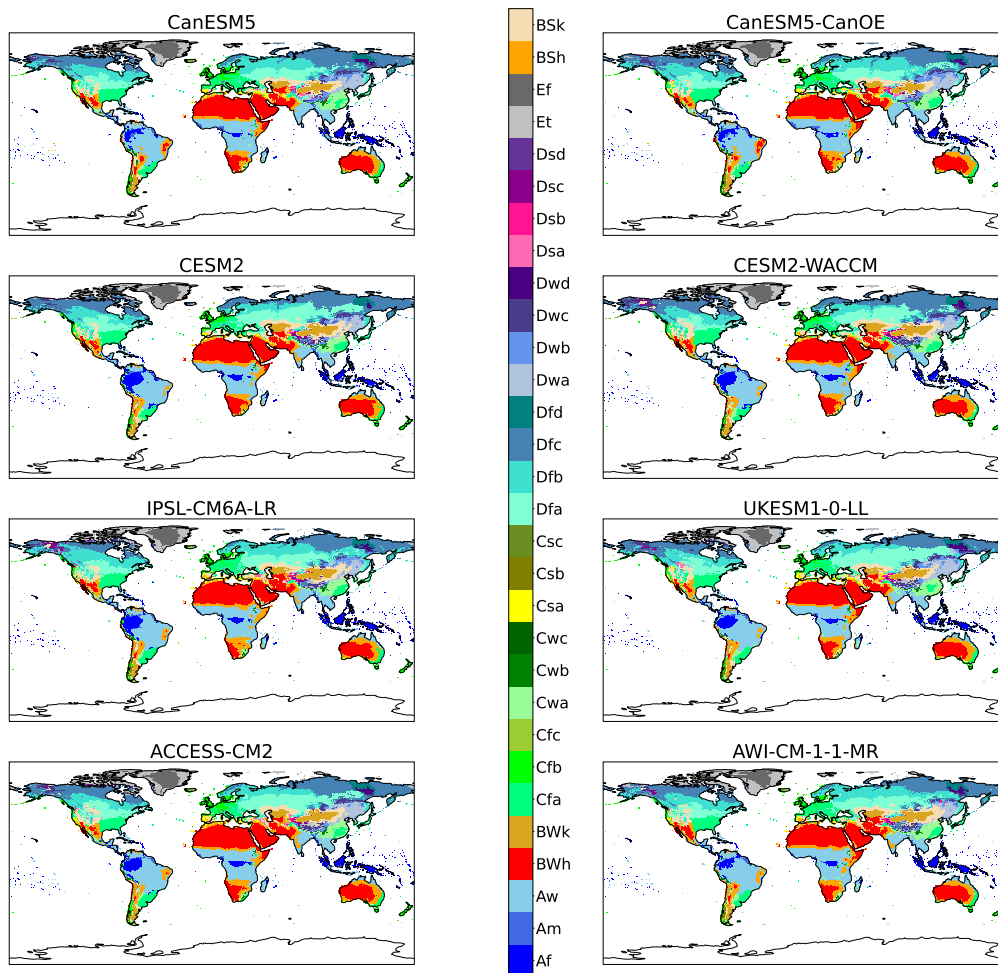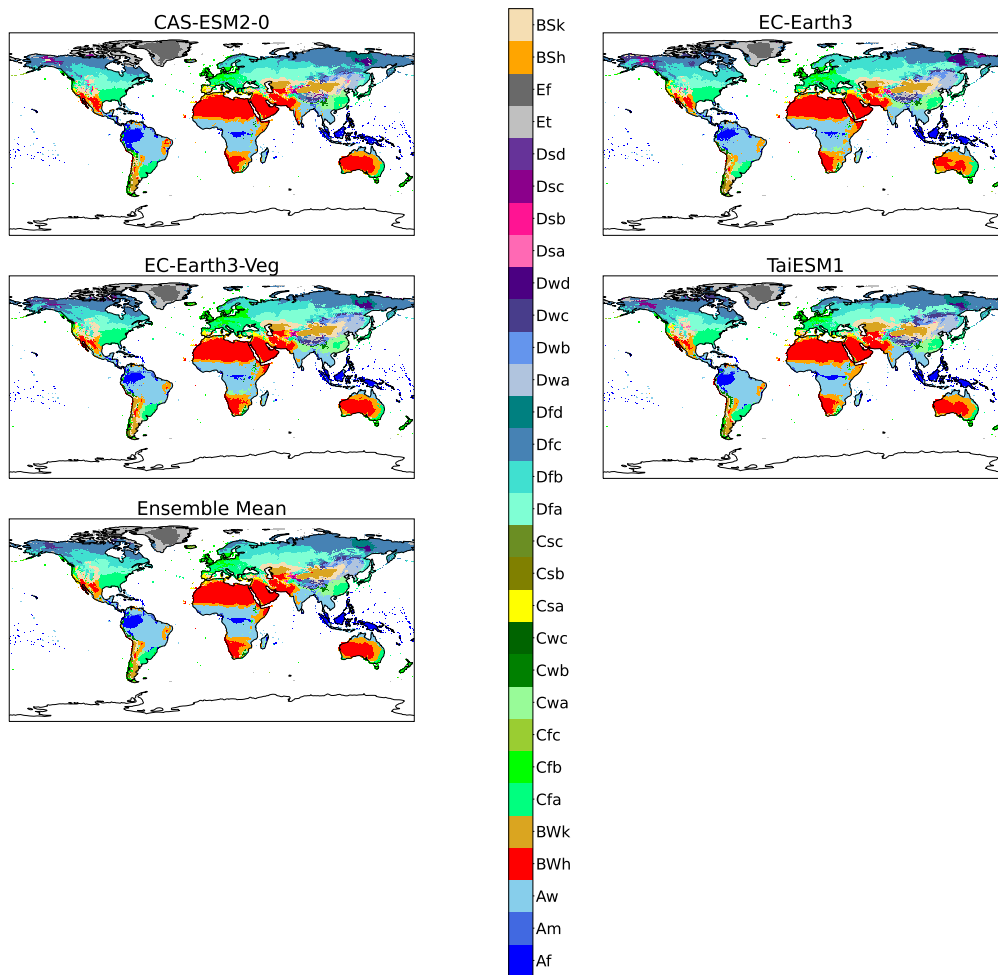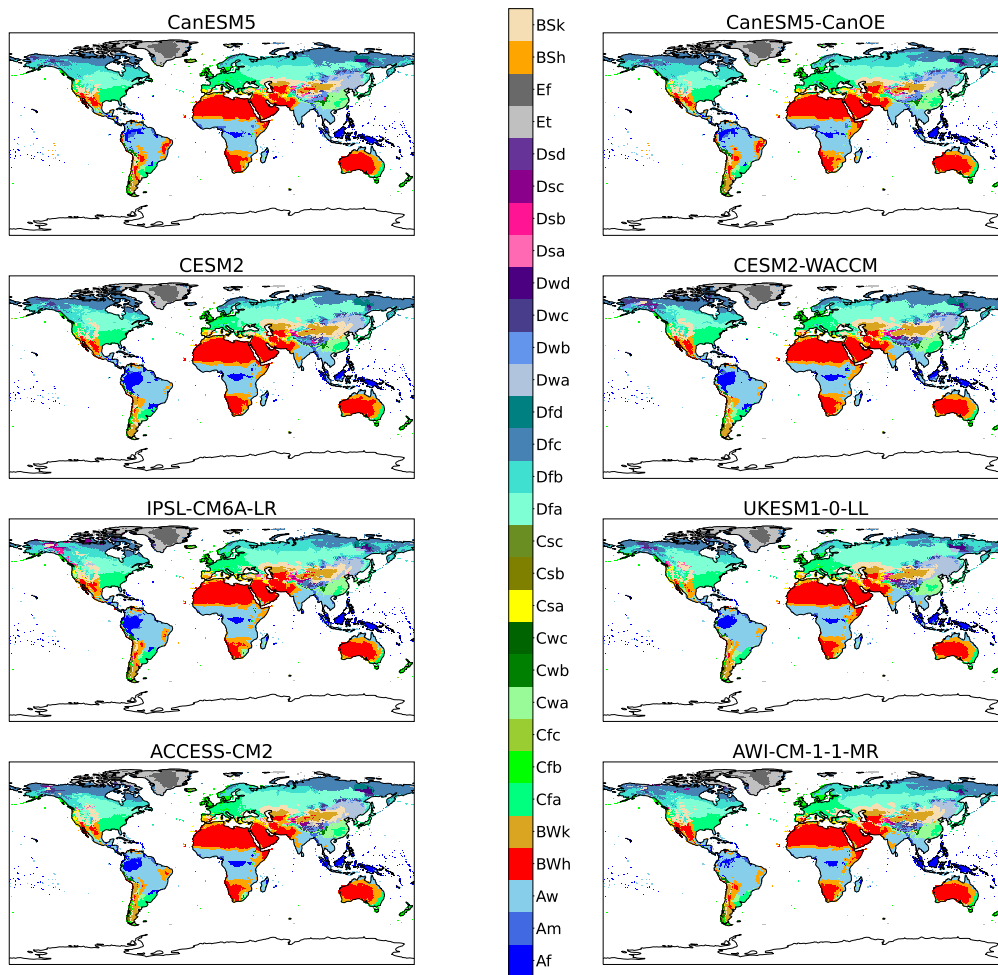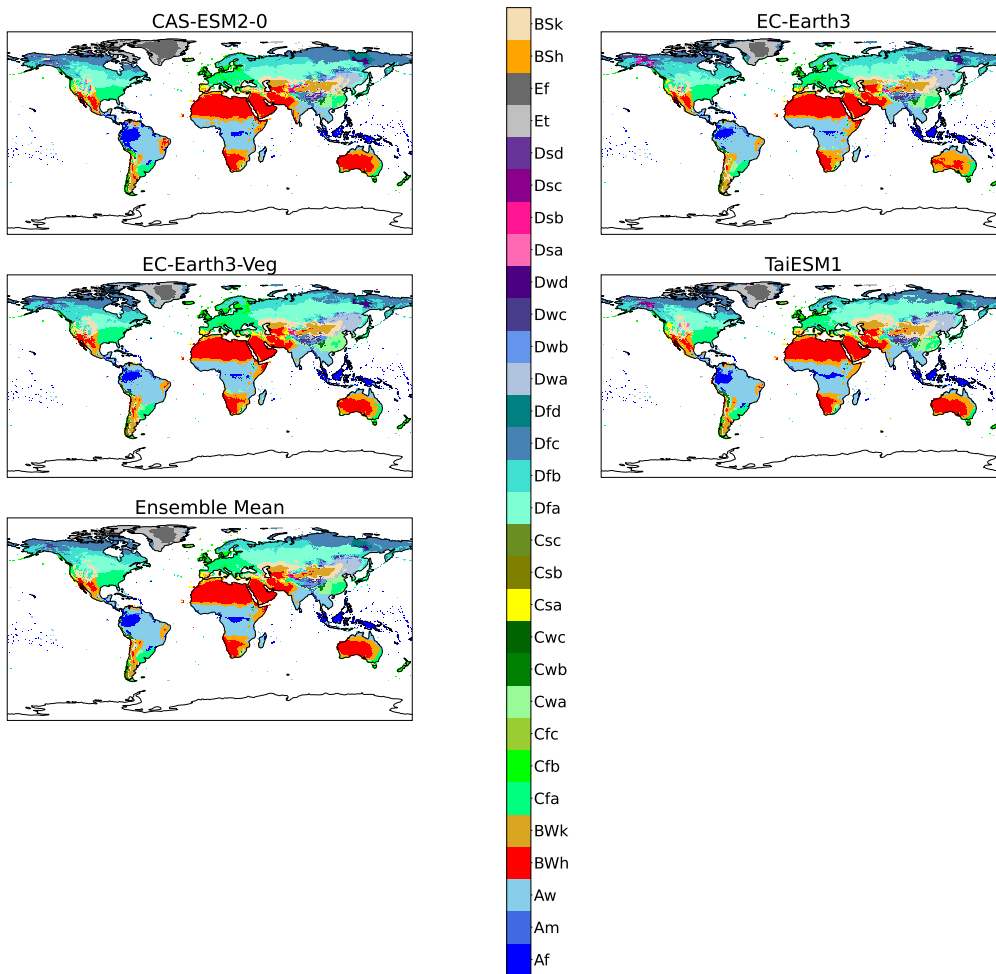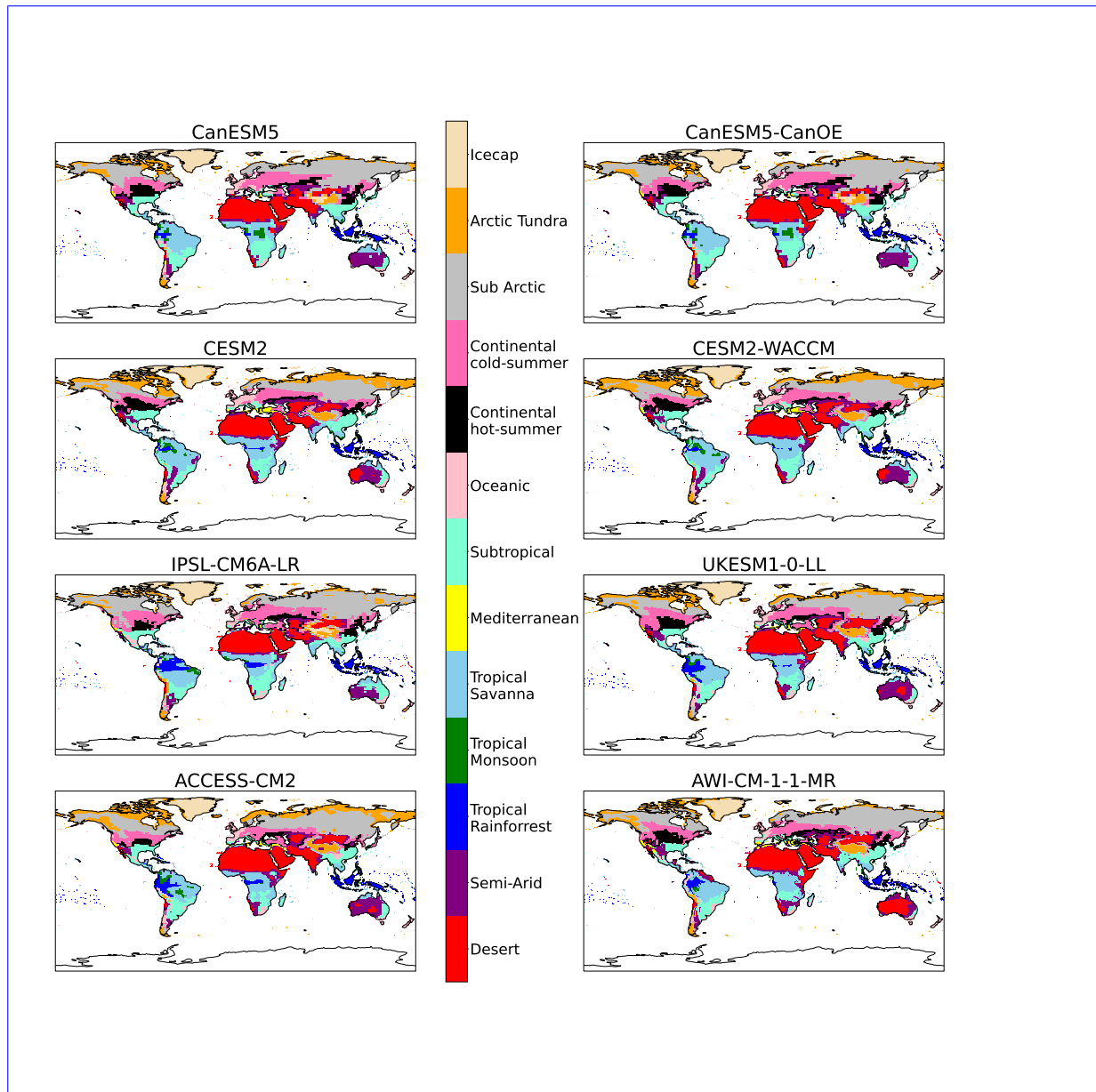
**Figure A3.** Continued.

**Figure A4.** ~~All models~~ Maps of KG classifications for each model at +~~1.5K~~ 2K, with anomaly correction.

**Figure A4.** Continued.

**Figure A5.** ~~All models~~ Maps of KG classifications for each model at +~~2K~~ 3K, with anomaly correction.

**Figure A5.** Continued.

**Figure A6.** ~~All models~~ Maps of KG classifications for each model at +~~3K~~ 4K, with anomaly correction.

**Figure A6.** Continued.

# Appendix B



**Figure B1.** Maps of streamlined KG classifications for each model for the reference period (1901 - 1931), without anomaly correction.
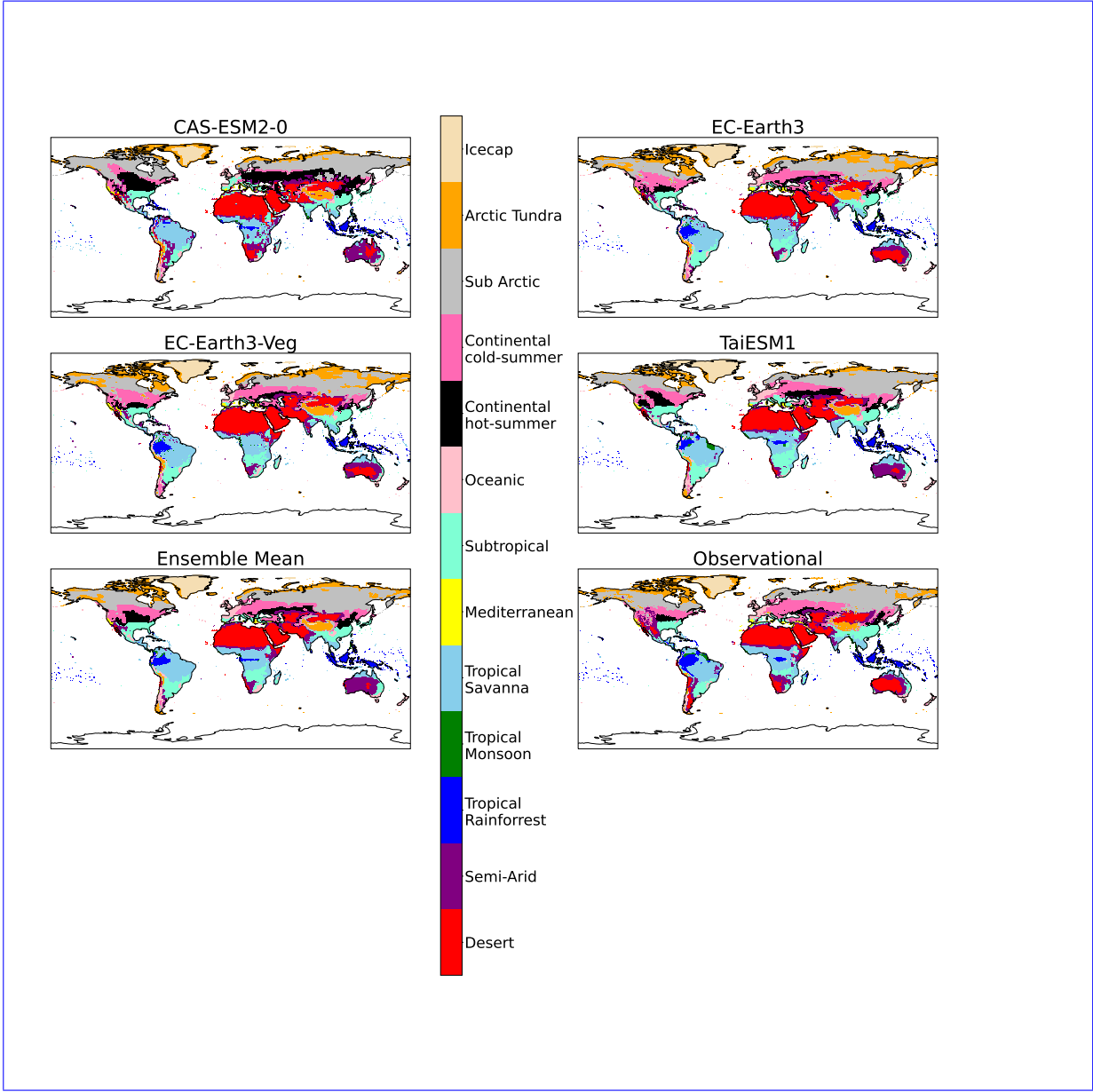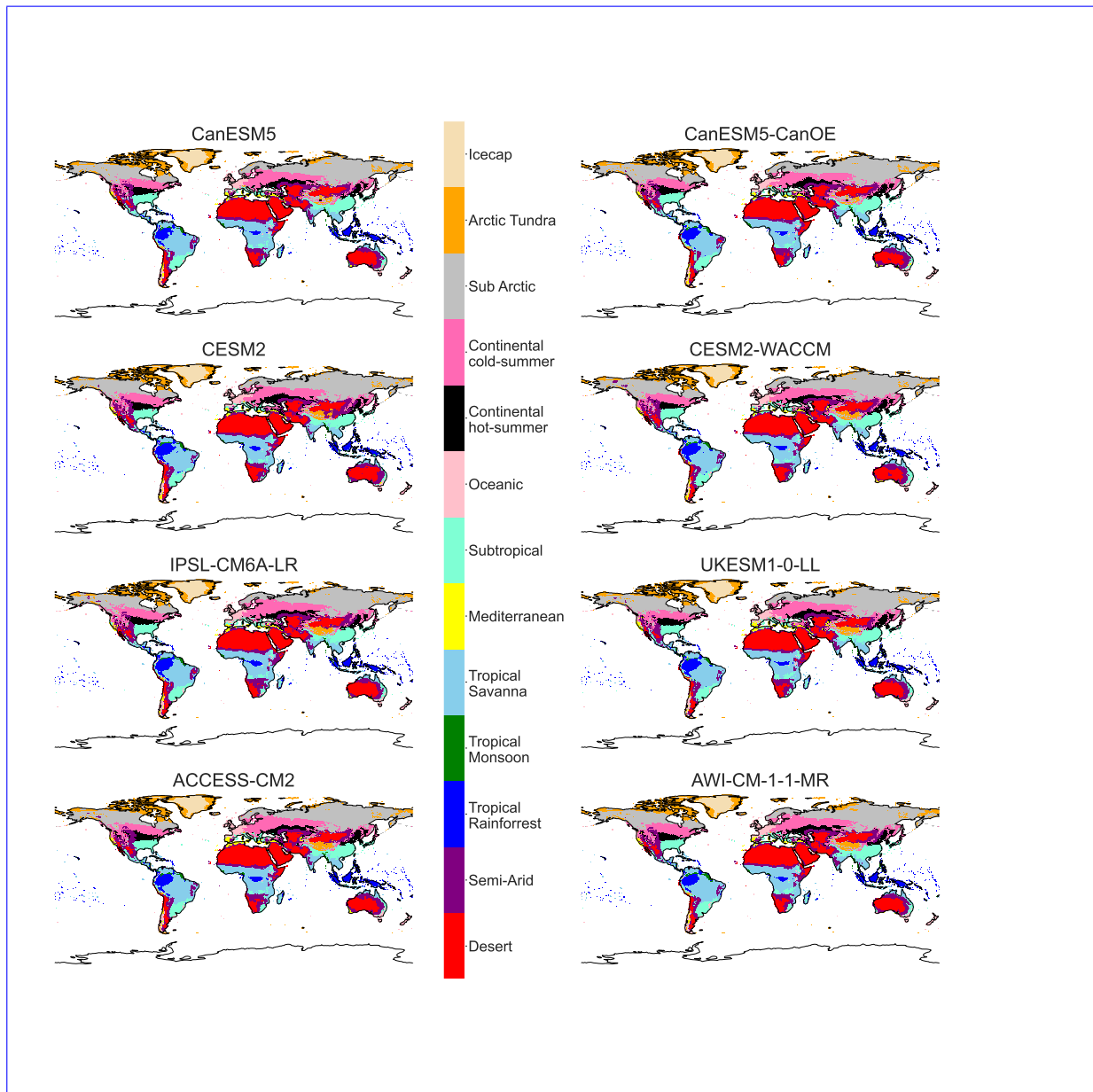
Figure B1. Continued.

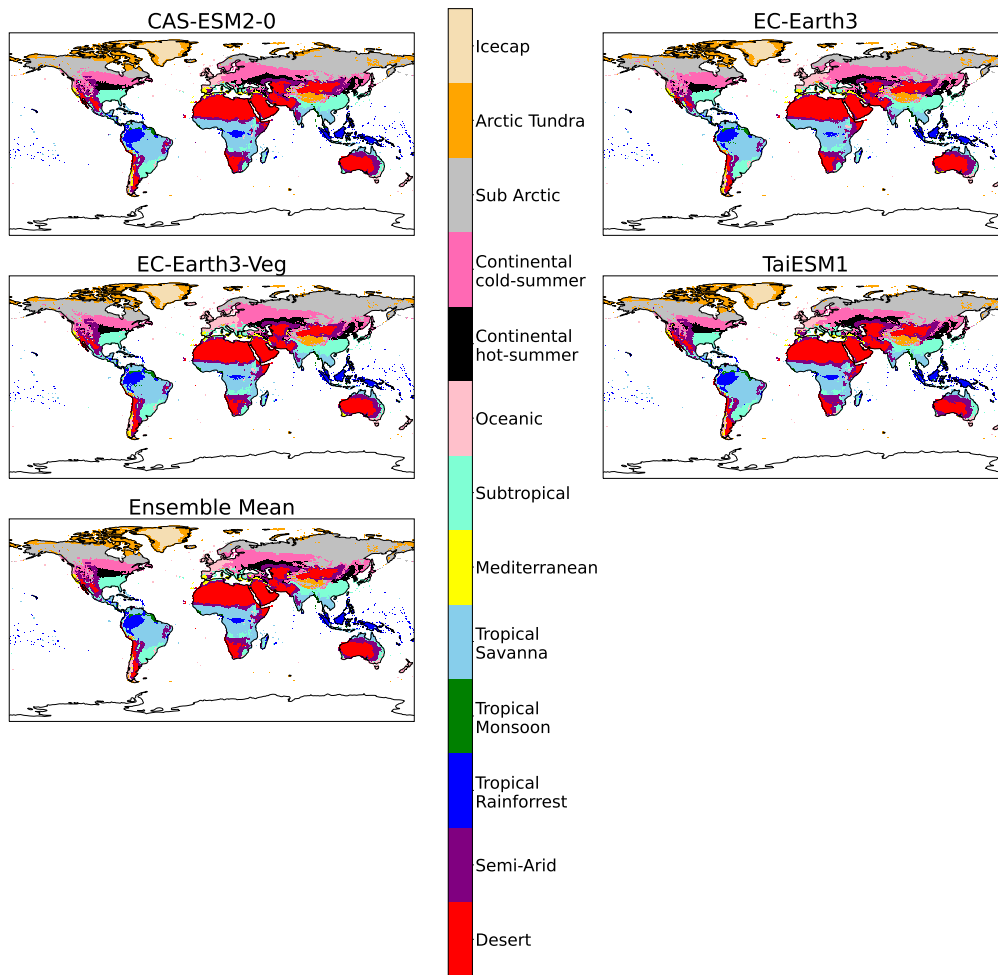**Figure B2.** ~~All models~~ Maps of streamlined KG classifications for each model at +~~4K~~ 1K, with anomaly correction.

CAS-ESM2-0

EC-Earth3

EC-Earth3-Veg

TaiESM1

Ensemble Mean

Icecap

Arctic Tundra

Sub Arctic

Continental cold-summer

Continental hot-summer

Oceanic

Subtropical

Mediterranean

Tropical Savanna

Tropical Monsoon

Tropical Rainforrest

Semi-Arid

Desert

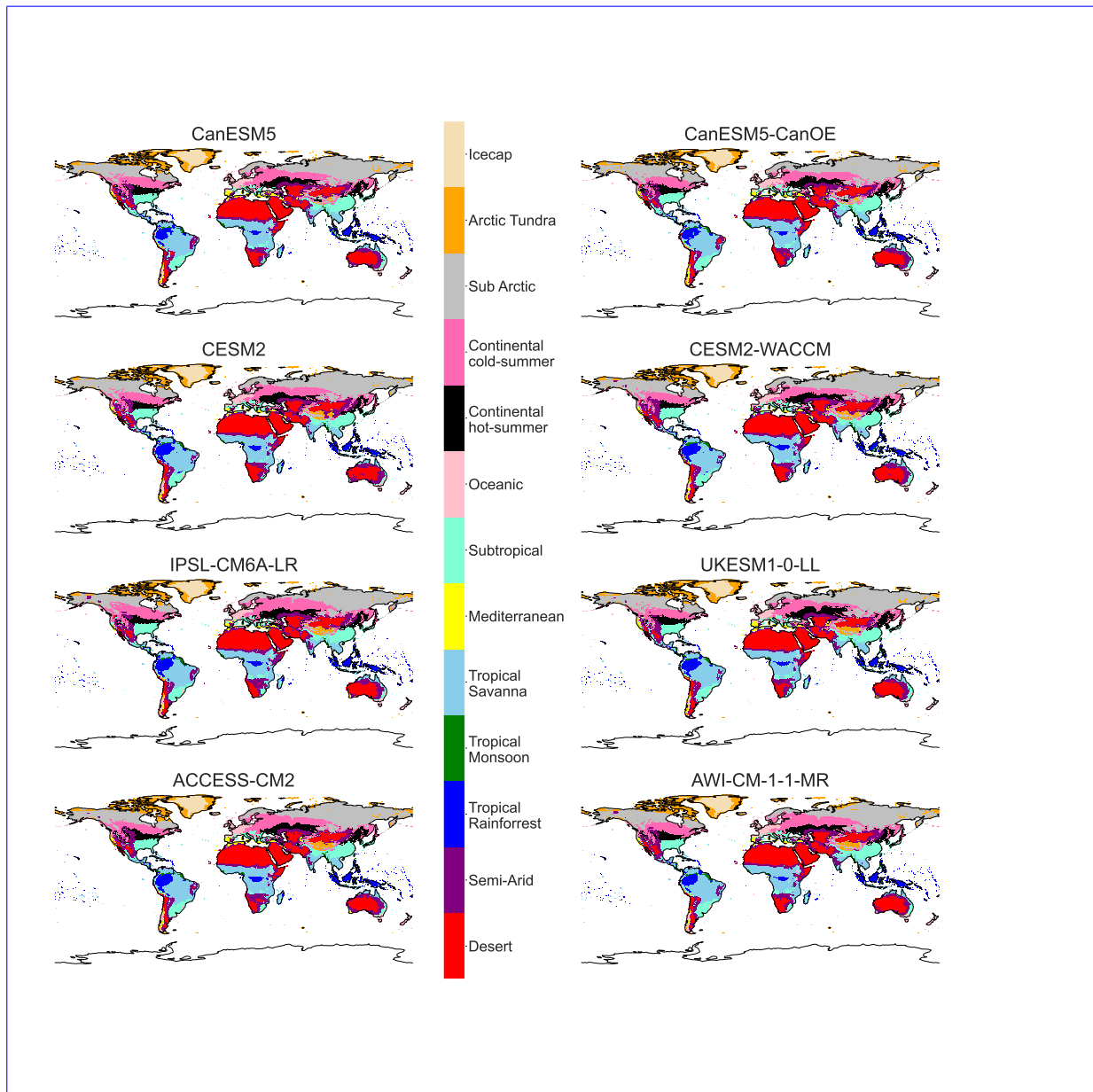**Figure B2.** Continued.

**Figure B3.** Maps of streamlined KG classifications for each model at +1.5K, with anomaly correction.

Figure B3. Continued.

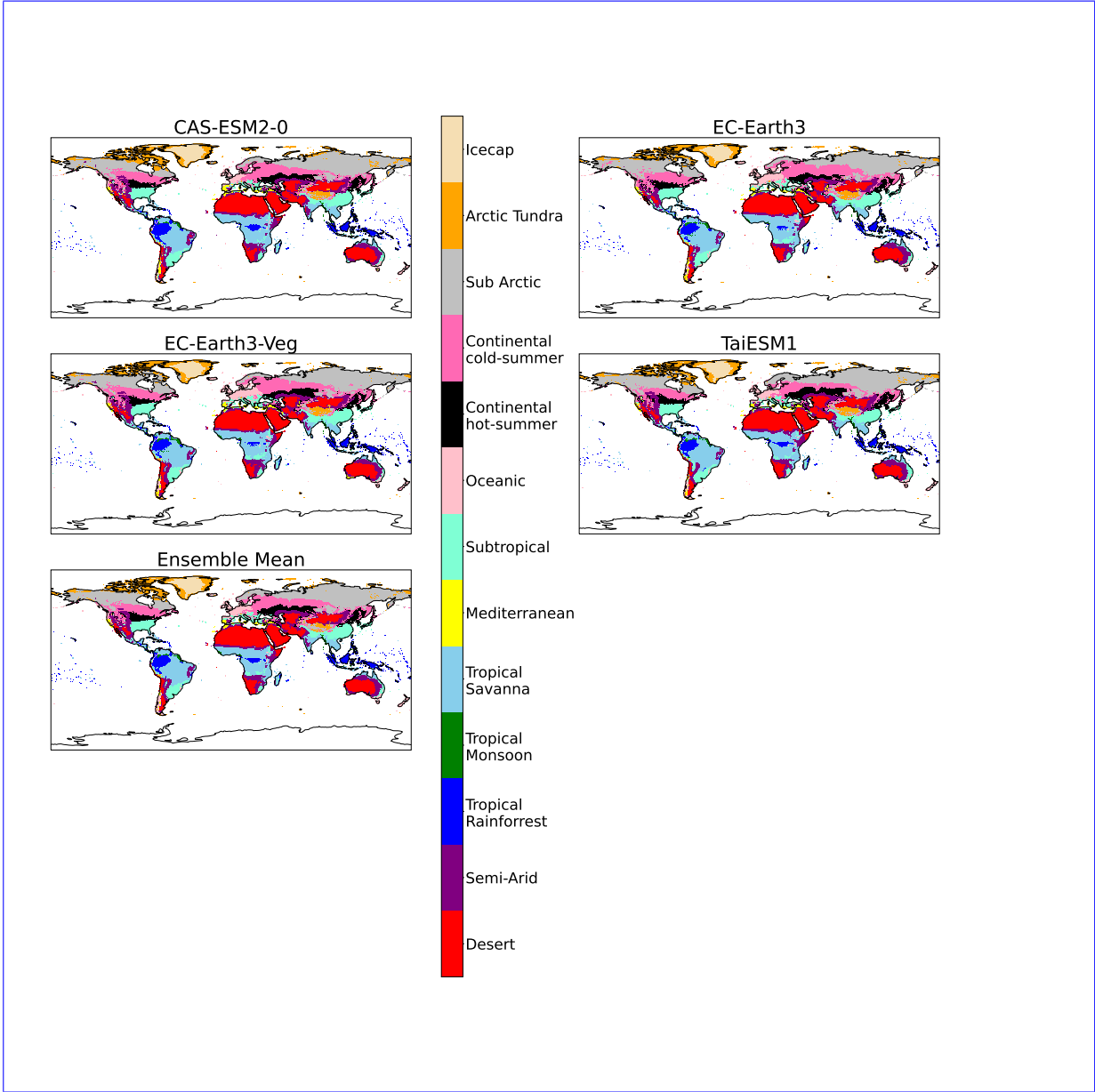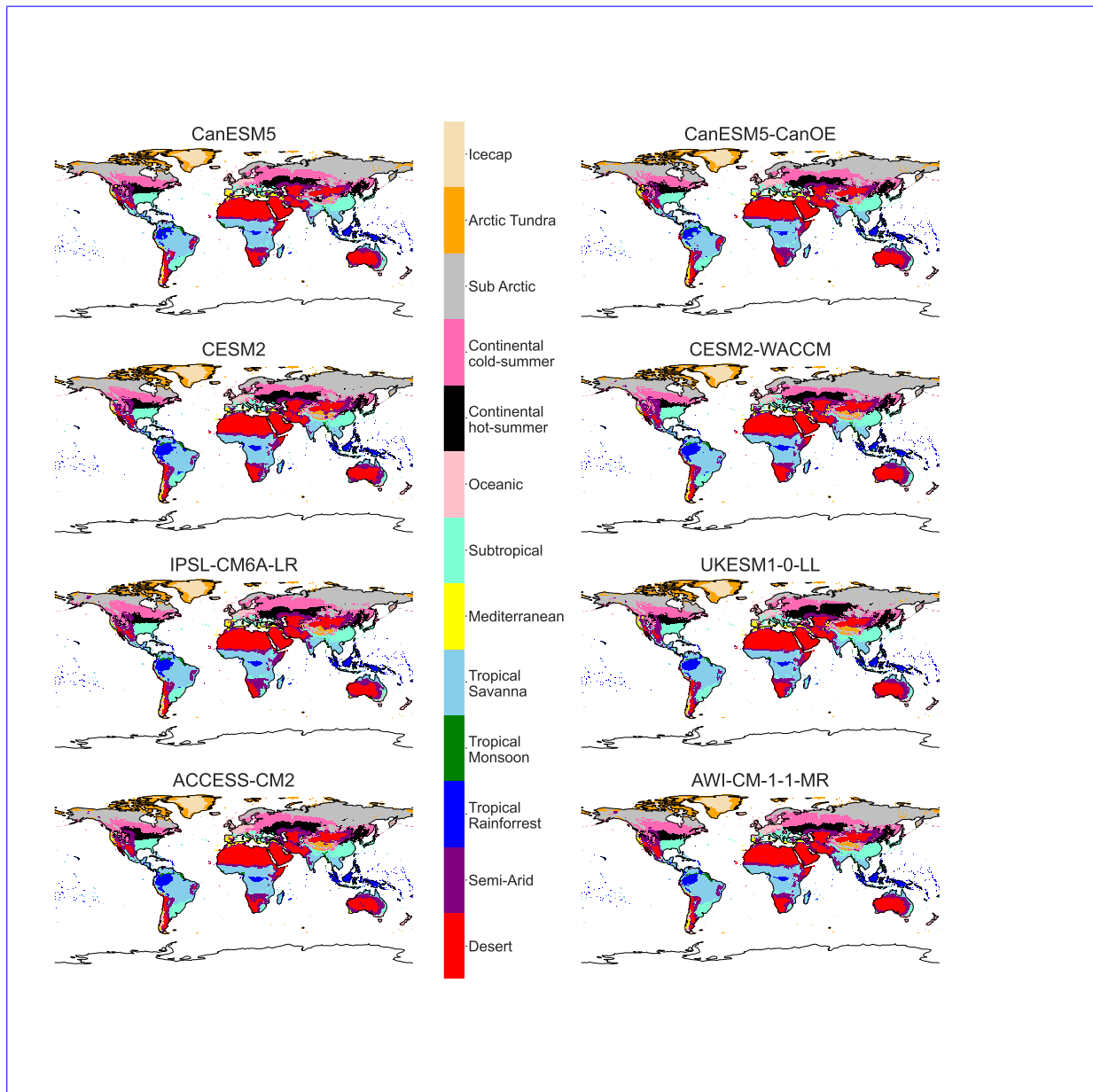**Figure B4.** Maps of streamlined KG classifications for each model at +2K, with anomaly correction.
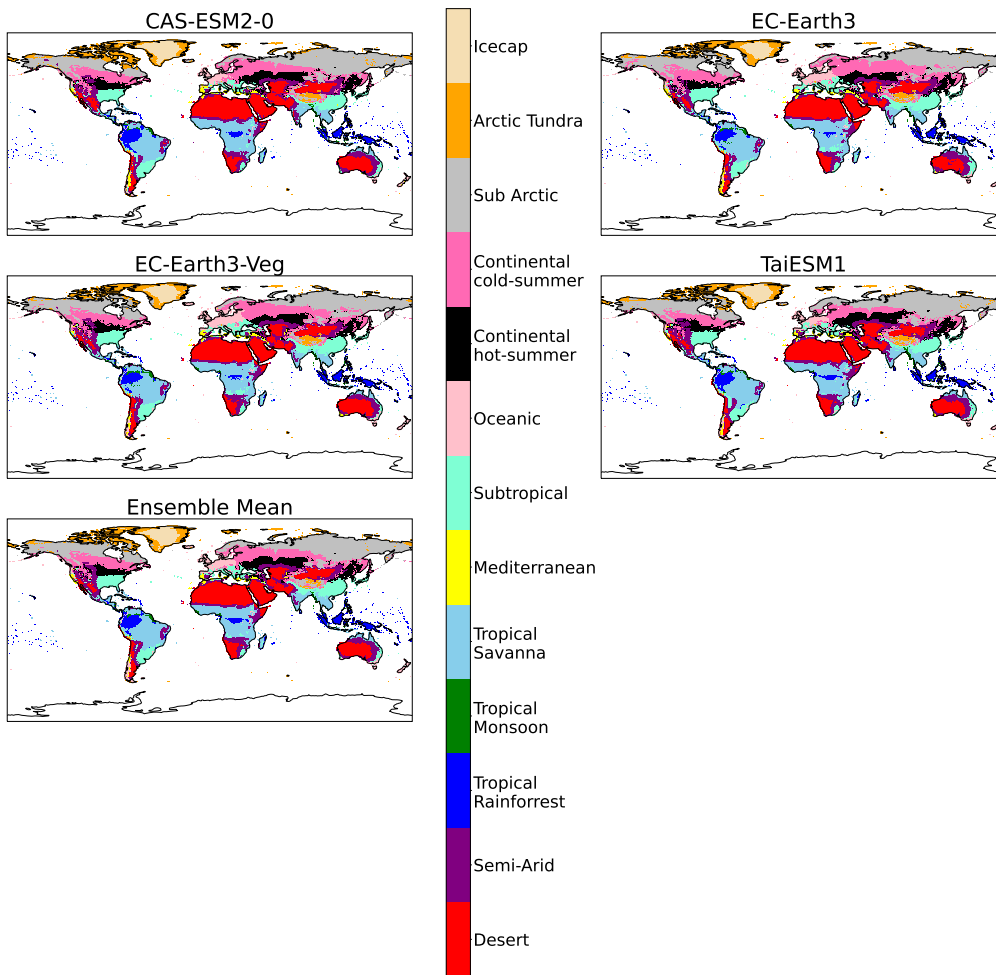
CAS-ESM2-0

EC-Earth3

EC-Earth3-Veg

TaiESM1

Ensemble Mean

Icecap

Arctic Tundra

Sub Arctic

Continental cold-summer

Continental hot-summer

Oceanic

Subtropical

Mediterranean

Tropical Savanna

Tropical Monsoon

Tropical Rainforrest

Semi-Arid

Desert

**Figure B4. Continued.**

**Figure B5.** Maps of streamlined KG classifications for each model at +3K, with anomaly correction.

CAS-ESM2-0

EC-Earth3

EC-Earth3-Veg

TaiESM1

Ensemble Mean

Icecap
Arctic Tundra
Sub Arctic
Continental cold-summer
Continental hot-summer
Oceanic
Subtropical
Mediterranean
Tropical Savanna
Tropical Monsoon
Tropical Rainforrest
Semi-Arid
Desert

**Figure B5.** Continued.

**Figure B6.** Maps of streamlined KG classifications for each model at +4K, with anomaly correction.
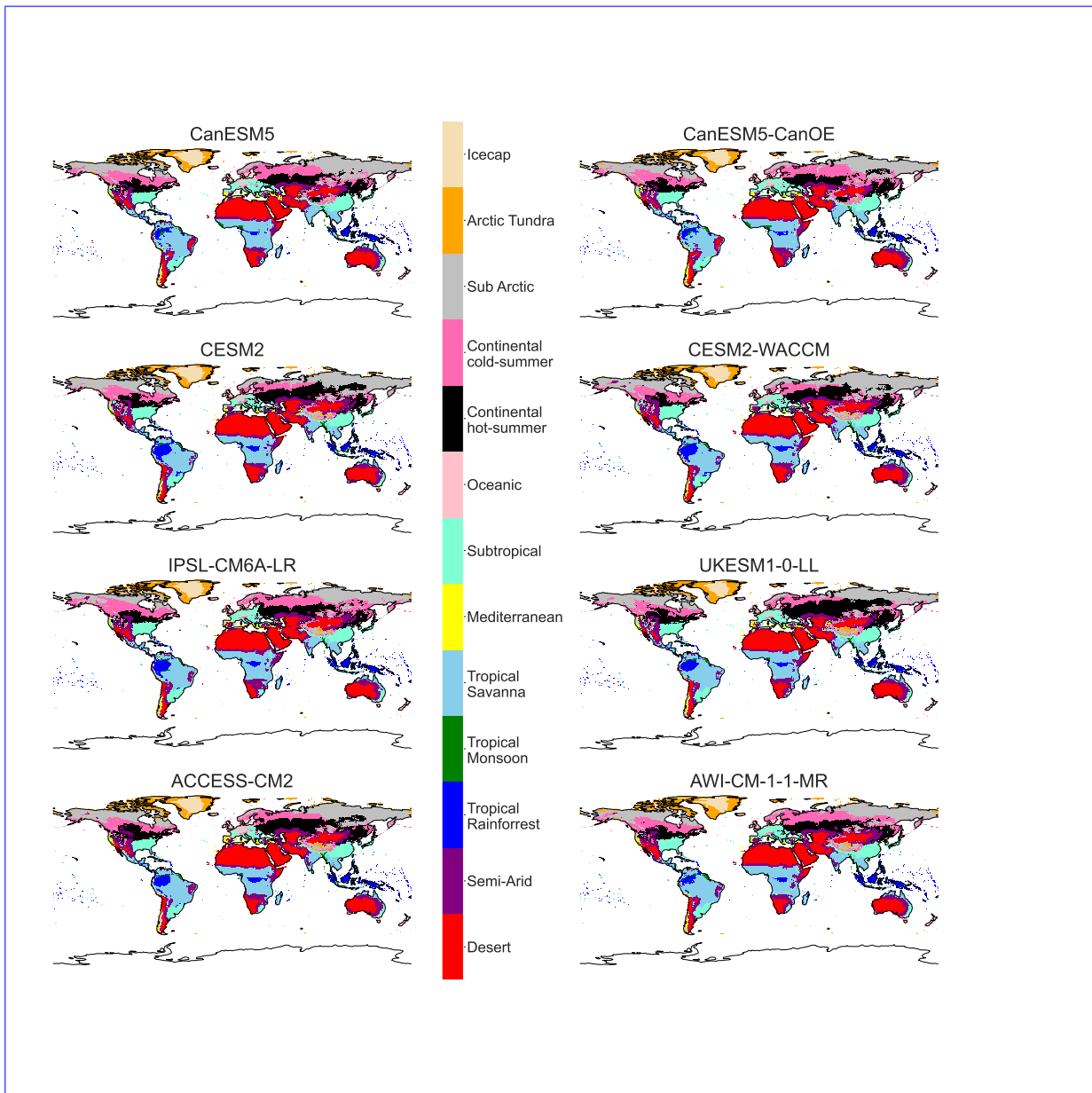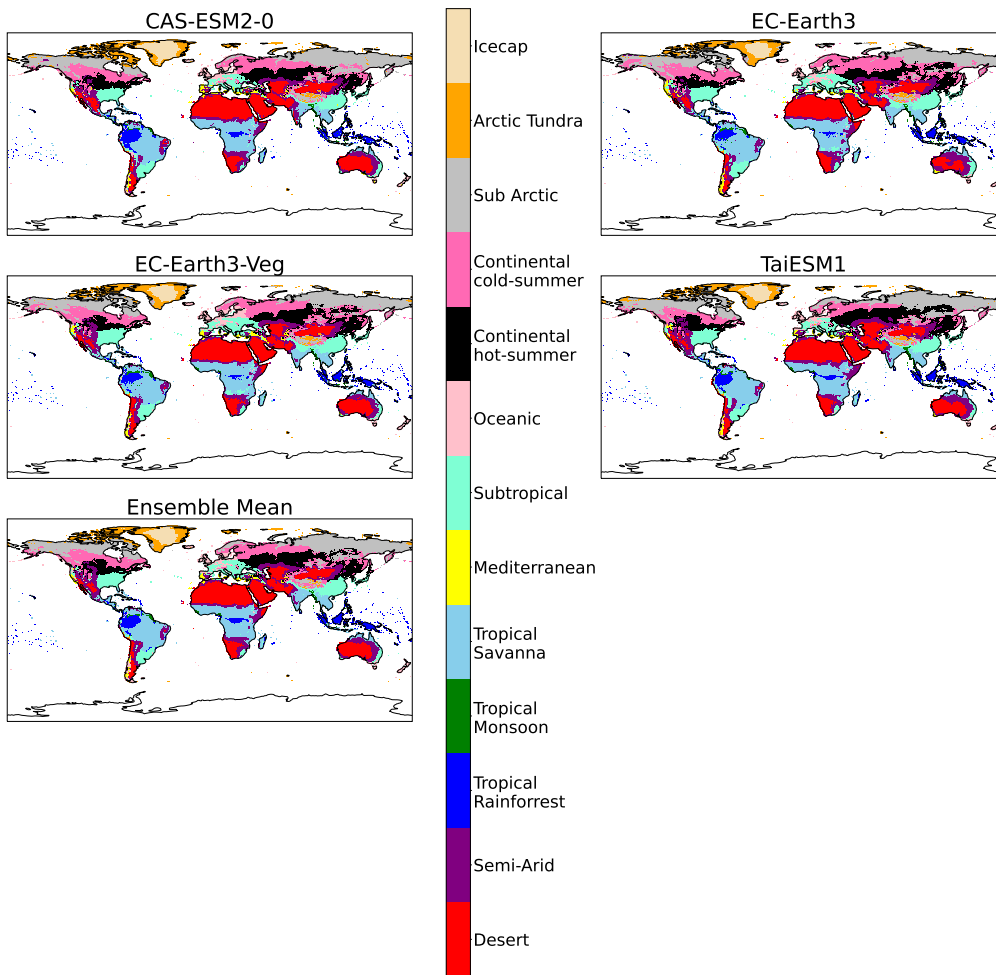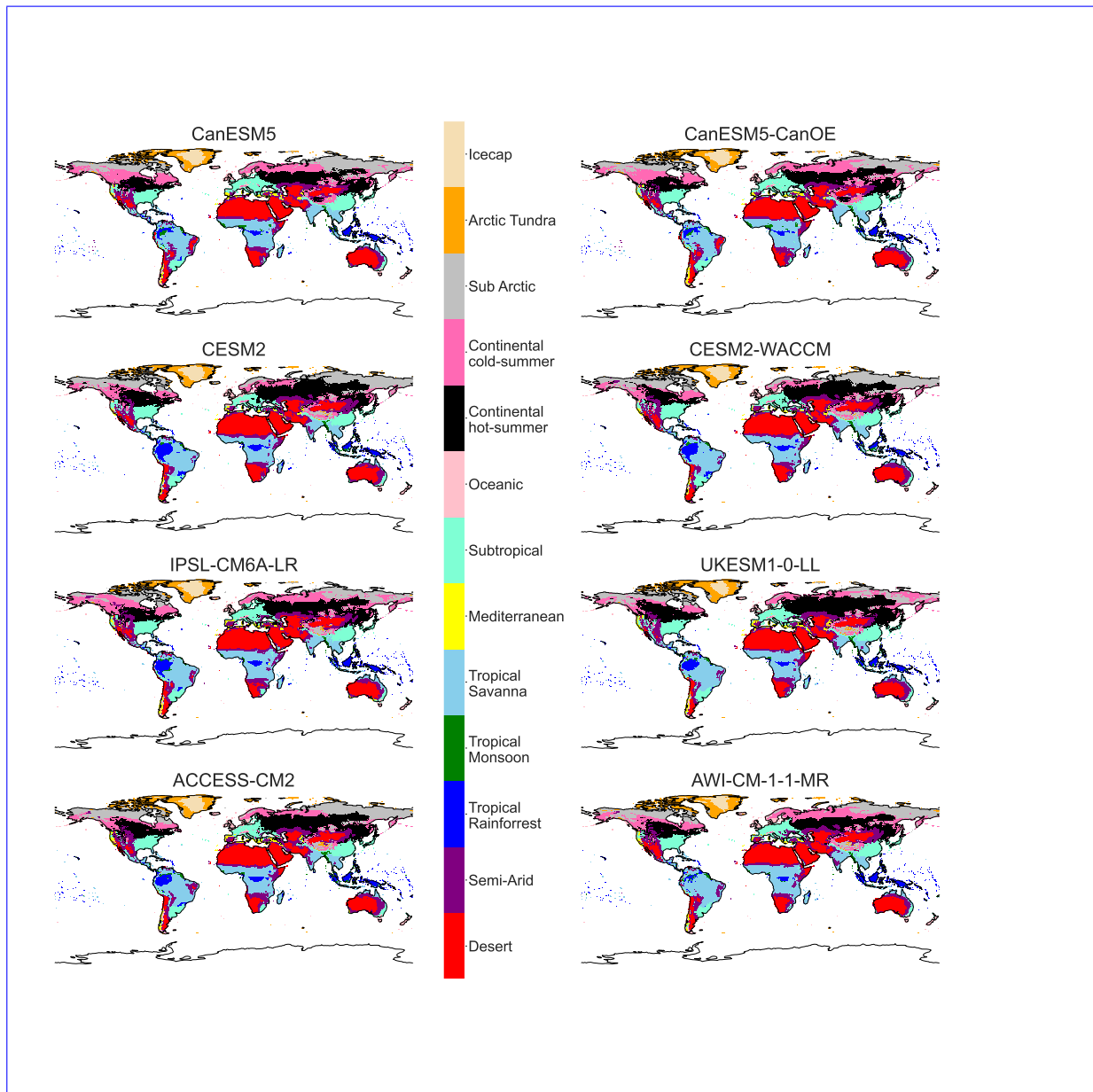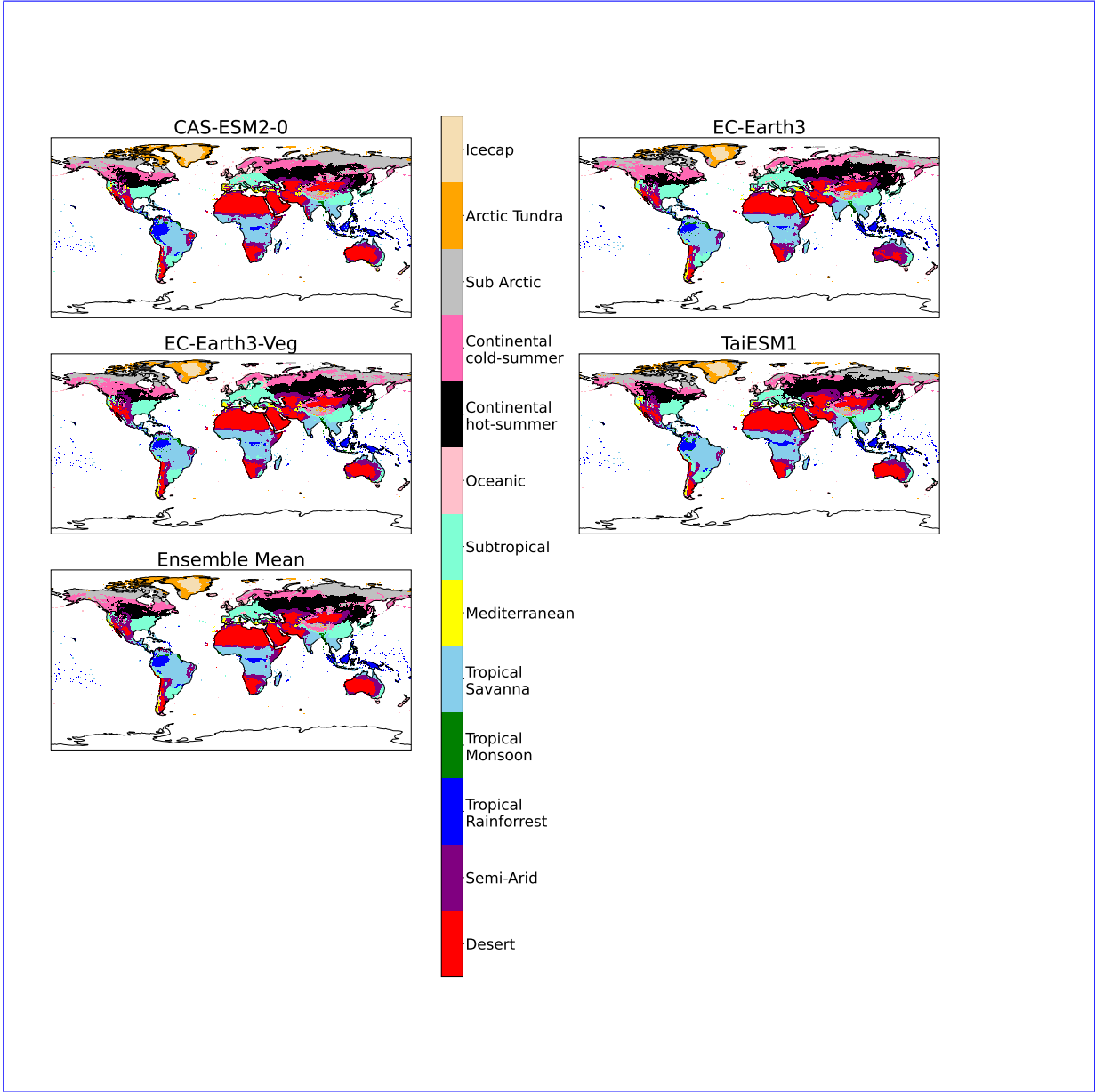
**Figure B6. Continued.**

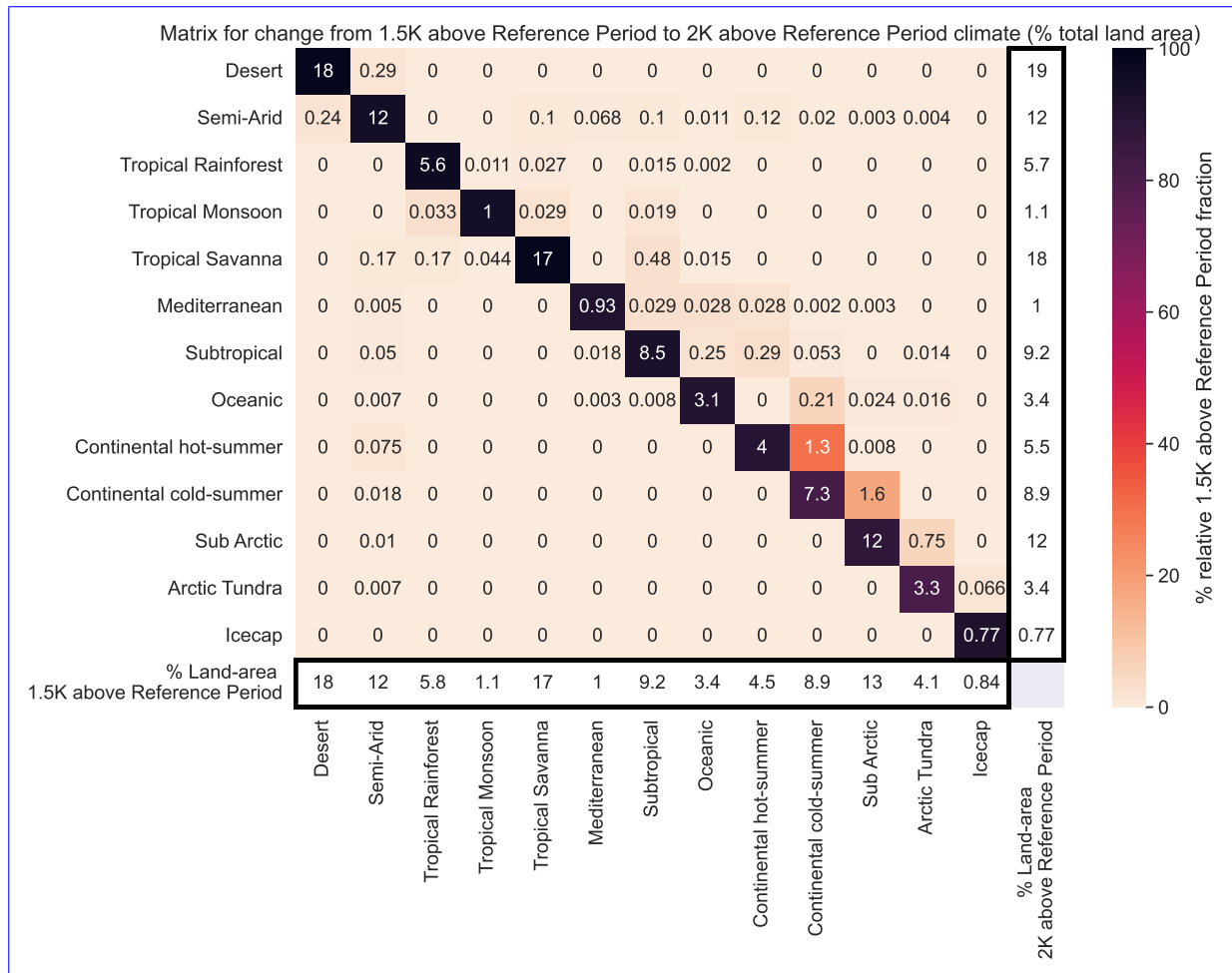**Figure C1.** Land area bioclimate classification change between 1.5K and 2K of global warming.

**Appendix D**
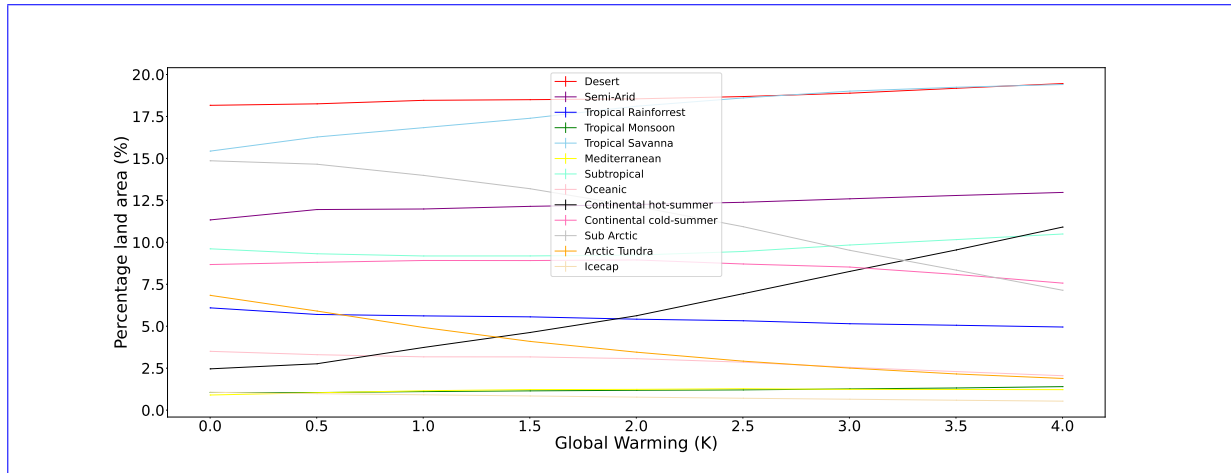


**Figure D1.** Land area distribution of individual streamlined classifications, Classifications that show large growth in their coverage include Continental hot-summer and Tropical Savanna. Classifications that show major reductions include Icecap, Arctic Tundra, and Sub Arctic.

*Author contributions.* MS carried out the data analysis and drafted the paper. MW & PC advised on the study. All authors contributed to the submitted paper.

*Competing interests.* No competing interests are present.

# References

CAS CAS-ESM1.0 model output prepared for CMIP6 ScenarioMIP ssp585, http://cera-www.dkrz.de/WDCC/meta/CMIP6/CMIP6.ScenarioMIP.CAS.CAS-ESM2-0.ssp585, 2018.

Beck, H. E., Zimmermann, N. E., McVicar, T. R., Vergopolan, N., Berg, A., and Wood, E. F.: Present and future Köppen-Geiger climate classification maps at 1-km resolution, Scientific Data, 5, 180 214, https://doi.org/10.1038/sdata.2018.214, 2018.

Boucher, O., Denvil, S., Levavasseur, G., Cozic, A., Caubel, A., Foujols, M.-A., Meurdesoif, Y., Cadule, P., Devilliers, M., Ghattas, J., Lebas, N., Lurton, T., Mellul, L., Musat, I., Mignot, J., and Cheruy, F.: IPSL IPSL-CM6A-LR model output prepared for CMIP6 CMIP historical, https://doi.org/10.22033/ESGF/CMIP6.5195, 2018.

Boucher, O., Denvil, S., Levavasseur, G., Cozic, A., Caubel, A., Foujols, M.-A., Meurdesoif, Y., Cadule, P., Devilliers, M., Dupont, E., and Lurton, T.: IPSL IPSL-CM6A-LR model output prepared for CMIP6 ScenarioMIP ssp585, https://doi.org/10.22033/ESGF/CMIP6.5271, 2019.

Chai, Z.: CAS CAS-ESM1.0 model output prepared for CMIP6 CMIP historical, https://doi.org/10.22033/ESGF/CMIP6.3353, 2020.

Cox, P., Huntingford, C., Nuttall, P., and Sparey, M.: Climate, Ticks and Disease, CABI, https://doi.org/10.1079/9781789249637.0003, 2021.

Danabasoglu, G.: NCAR CESM2 model output prepared for CMIP6 ScenarioMIP ssp585, https://doi.org/10.22033/ESGF/CMIP6.7768, 2019a.

Danabasoglu, G.: NCAR CESM2 model output prepared for CMIP6 CMIP historical, https://doi.org/10.22033/ESGF/CMIP6.7627, 2019b.

Danabasoglu, G.: NCAR CESM2-WACCM model output prepared for CMIP6 CMIP historical, https://doi.org/10.22033/ESGF/CMIP6.10071, 2019c.

Danabasoglu, G.: NCAR CESM2-WACCM model output prepared for CMIP6 ScenarioMIP ssp585, https://doi.org/10.22033/ESGF/CMIP6.10115, 2019d.

Danek, C., Shi, X., Stepanek, C., Yang, H., Barbi, D., Hegewald, J., and Lohmann, G.: AWI AWI-ESM1.1LR model output prepared for CMIP6 CMIP historical, https://doi.org/10.22033/ESGF/CMIP6.9328, 2020.

Dix, M., Bi, D., Dobrohotoff, P., Fiedler, R., Harman, I., Law, R., Mackallah, C., Marsland, S., O'Farrell, S., Rashid, H., Srbinovsky, J., Sullivan, A., Trenham, C., Vohralik, P., Watterson, I., Williams, G., Woodhouse, M., Bodman, R., Dias, F. B., Domingues, C. M., Hannah, N., Heerdegen, A., Savita, A., Wales, S., Allen, C., Druken, K., Evans, B., Richards, C., Ridzwan, S. M., Roberts, D., Smillie, J., Snow, K., Ward, M., and Yang, R.: CSIRO-ARCCSS ACCESS-CM2 model output prepared for CMIP6 ScenarioMIP ssp585, https://doi.org/10.22033/ESGF/CMIP6.4332, 2019a.

Dix, M., Bi, D., Dobrohotoff, P., Fiedler, R., Harman, I., Law, R., Mackallah, C., Marsland, S., O'Farrell, S., Rashid, H., Srbinovsky, J., Sullivan, A., Trenham, C., Vohralik, P., Watterson, I., Williams, G., Woodhouse, M., Bodman, R., Dias, F. B., Domingues, C. M., Hannah, N., Heerdegen, A., Savita, A., Wales, S., Allen, C., Druken, K., Evans, B., Richards, C., Ridzwan, S. M., Roberts, D., Smillie, J., Snow, K., Ward, M., and Yang, R.: CSIRO-ARCCSS ACCESS-CM2 model output prepared for CMIP6 CMIP historical, https://doi.org/10.22033/ESGF/CMIP6.4271, 2019b.

EC-Earth-Consortium: EC-Earth-Consortium EC-Earth3 model output prepared for CMIP6 ScenarioMIP ssp585, https://doi.org/10.22033/ESGF/CMIP6.4912, 2019a.

EC-Earth-Consortium: EC-Earth-Consortium EC-Earth3 model output prepared for CMIP6 CMIP historical, https://doi.org/10.22033/ESGF/CMIP6.4700, 2019b.

EC-Earth-Consortium: EC-Earth-Consortium EC-Earth3-Veg model output prepared for CMIP6 ScenarioMIP ssp585, https://doi.org/10.22033/ESGF/CMIP6.4914, 2019c.

EC-Earth-Consortium: EC-Earth-Consortium EC-Earth3-Veg model output prepared for CMIP6 CMIP historical, https://doi.org/10.22033/ESGF/CMIP6.4706, 2019d.

Every, J. P., Li, L., and Dorrell, D. G.: Köppen-Geiger climate classification adjustment of the BRL diffuse irradiation model for Australian locations, Renewable Energy, 147, 2453–2469, https://doi.org/10.1016/j.renene.2019.09.114, 2020.

Eyring, V., Bony, S., Meehl, G. A., Senior, C. A., Stevens, B., Stouffer, R. J., and Taylor, K. E.: Overview of the Coupled Model Intercomparison Project Phase 6 (CMIP6) experimental design and organization, Geoscientific Model Development, 9, 1937–1958, https://doi.org/10.5194/gmd-9-1937-2016, 2016.

Feng, S., Hu, Q., Huang, W., Ho, C.-H., Li, R., and Tang, Z.: Projected climate regime shift under future global warming from multi-model, multi-scenario CMIP5 simulations, Global and Planetary Change, 112, 41–52, https://doi.org/https://doi.org/10.1016/j.gloplacha.2013.11.002, 2014.

Good, P., Sellar, A., Tang, Y., Rumbold, S., Ellis, R., Kelley, D., and Kuhlbrodt, T.: MOHC UKESM1.0-LL model output prepared for CMIP6 ScenarioMIP ssp585, https://doi.org/10.22033/ESGF/CMIP6.6405, 2019.

Harris, I., Osborn, T., Jones, P., and Lister, D.: Version 4 of the CRU TS monthly high-resolution gridded multivariate climate dataset, Scientific Data, 7, https://doi.org/10.1038/s41597-020-0453-3, 2020.

Kim, J.-B. and Bae, D.-H.: The Impacts of Global Warming on Climate Zone Changes Over Asia Based on CMIP6 Projections, Earth and Space Science, 8, e2021EA001 701, https://doi.org/10.1029/2021EA001701, 2021.

Kottek, M., Grieser, J., Beck, C., Rudolf, B., and Rubel, F.: World Map of the Köppen-Geiger Climate Classification Updated, Meteorologische Zeitschrift, 15, 259–263, https://doi.org/10.1127/0941-2948/2006/0130, 2006.

Köppen, W.: Die Wärmezonen der Erde, nach der Dauer der heissen, gemässigten und kalten Zeit und nach der Wirkung der Wärme auf die organische Welt betrachtet., Meteor. Z., 1, 215–226, https://doi.org/10.1007/s11367-013-0693-y, 1884.

Köppen, W.: Das geographische System der Klimate,, Gebrüder Borntraeger, pp. 1–44, 1936.

Lee, W.-L. and Liang, H.-C.: AS-RCEC TaiESM1.0 model output prepared for CMIP6 ScenarioMIP ssp585, https://doi.org/10.22033/ESGF/CMIP6.9823, 2020a.

Lee, W.-L. and Liang, H.-C.: AS-RCEC TaiESM1.0 model output prepared for CMIP6 CMIP historical, https://doi.org/10.22033/ESGF/CMIP6.9755, 2020b.

Lugo, A. E., Brown, S. L., Dodson, R., Smith, T. S., and Shugart, H. H.: The Holdridge life zones of the conterminous United States in relation to ecosystem mapping, Journal of Biogeography, 26, 1025–1038, https://doi.org/10.1046/j.1365-2699.1999.00329.x, 1999.

Masson-Delmotte, V., Zhai, P., Pirani, A., Connors, S., Péan, C., Berger, S., Caud, N., Chen, Y., Goldfarb, L., Gomis, M., Huang, M., Leitzell, K., Lonnoy, E., Matthews, J., Maycock, T., Waterfield, T., Yelekçi, O., Yu, R., and Zhou, B. e.: Summary for Policymakers., In: Climate Change 2021: The Physical Science Basis. Contribution of Working Group I to the Sixth Assessment Report of the Intergovernmental Panel on Climate Change., IPCC, Cambridge University Press., 2021.

Nijsse, F. J. M. M., Cox, P. M., and Williamson, M. S.: Emergent constraints on transient climate response (TCR) and equilibrium climate sensitivity (ECS) from historical warming in CMIP5 and CMIP6 models, Earth System Dynamics, 11, 737–750, https://doi.org/10.5194/esd-11-737-2020, 2020.

Paris-Agreement: Paris Agreement.

Peel, M. C., McMahon, T. A., Finlayson, B. L., and Watson, F. G.: Identification and explanation of continental differences in the variability of annual runoff, Journal of Hydrology, 250, 224–240, https://doi.org/10.1016/S0022-1694(01)00438-3, 2001.

Peel, M. C., Finlayson, B. L., and McMahon, T. A.: Updated world map of the Köppen-Geiger climate classification, Hydrology and Earth System Sciences, 11, 1633–1644, https://doi.org/10.5194/hess-11-1633-2007, 2007.

330   Phillips, T. J. and Bonfils, C. J. W.: Köppen bioclimatic evaluation of CMIP historical climate simulations, Environmental Research Letters, 10, 064 005, https://doi.org/10.1088/1748-9326/10/6/064005, 2015.

Pörtner, H.-O., Roberts, D., Poloczanska, E., Mintenbeck, K., Tignor, M., Alegría, A., Craig, M., Langsdorf, S., S., L., Möller, V., and Okem, A. e.: Summary for Policymakers., In: Climate Change 2022: Impacts, Adaptation, and Vulnerability. Contribution of Working Group II to the Sixth Assessment Report of the Intergovernmental Panel on Climate Change., IPCC, Cambridge University Press., 2022.

335   Rahimi, J., Laux, P., and Khalili, A.: Assessment of climate change over Iran: CMIP5 results and their presentation in terms of Köppen–Geiger climate zones, Theoretical and Applied Climatology, 141, https://doi.org/10.1007/s00704-020-03190-8, 2020.

Russell, R. J.: Dry climates of the United States, University of California publications in geography, University of California Press, 1931.

Semmler, T., Danilov, S., Rackow, T., Sidorenko, D., Barbi, D., Hegewald, J., Pradhan, H. K., Sein, D., Wang, Q., and Jung, T.: AWI AWI-CM1.1MR model output prepared for CMIP6 ScenarioMIP ssp585, https://doi.org/10.22033/ESGF/CMIP6.2817, 2019.

340   Sherwood, S. C., Webb, M. J., Annan, J. D., Armour, K. C., Forster, P. M., Hargreaves, J. C., Hegerl, G., Klein, S. A., Marvel, K. D., Rohling, E. J., Watanabe, M., Andrews, T., Braconnot, P., Bretherton, C. S., Foster, G. L., Hausfather, Z., von der Heydt, A. S., Knutti, R., Mauritsen, T., Norris, J. R., Proistosescu, C., Rugenstein, M., Schmidt, G. A., Tokarska, K. B., and Zelinka, M. D.: An Assessment of Earth's Climate Sensitivity Using Multiple Lines of Evidence, Reviews of Geophysics, 58, e2019RG000 678, https://doi.org/10.1029/2019RG000678, 2020.

345   Swart, N. C., Cole, J. N., Kharin, V. V., Lazare, M., Scinocca, J. F., Gillett, N. P., Anstey, J., Arora, V., Christian, J. R., Jiao, Y., Lee, W. G., Majaess, F., Saenko, O. A., Seiler, C., Seinen, C., Shao, A., Solheim, L., von Salzen, K., Yang, D., Winter, B., and Sigmond, M.: CCCma CanESM5 model output prepared for CMIP6 ScenarioMIP ssp585, https://doi.org/10.22033/ESGF/CMIP6.3696, 2019a.

Swart, N. C., Cole, J. N., Kharin, V. V., Lazare, M., Scinocca, J. F., Gillett, N. P., Anstey, J., Arora, V., Christian, J. R., Jiao, Y., Lee, W. G., Majaess, F., Saenko, O. A., Seiler, C., Seinen, C., Shao, A., Solheim, L., von Salzen, K., Yang, D., Winter, B., and Sigmond, M.: CCCma

350   CanESM5-CanOE model output prepared for CMIP6 ScenarioMIP ssp585, https://doi.org/10.22033/ESGF/CMIP6.10276, 2019b.

Swart, N. C., Cole, J. N., Kharin, V. V., Lazare, M., Scinocca, J. F., Gillett, N. P., Anstey, J., Arora, V., Christian, J. R., Jiao, Y., Lee, W. G., Majaess, F., Saenko, O. A., Seiler, C., Seinen, C., Shao, A., Solheim, L., von Salzen, K., Yang, D., Winter, B., and Sigmond, M.: CCCma CanESM5-CanOE model output prepared for CMIP6 CMIP historical, https://doi.org/10.22033/ESGF/CMIP6.10260, 2019c.

Swart, N. C., Cole, J. N., Kharin, V. V., Lazare, M., Scinocca, J. F., Gillett, N. P., Anstey, J., Arora, V., Christian, J. R., Jiao, Y., Lee, W. G.,

355   Majaess, F., Saenko, O. A., Seiler, C., Seinen, C., Shao, A., Solheim, L., von Salzen, K., Yang, D., Winter, B., and Sigmond, M.: CCCma CanESM5 model output prepared for CMIP6 CMIP historical, https://doi.org/10.22033/ESGF/CMIP6.3610, 2019d.

Tang, Y., Rumbold, S., Ellis, R., Kelley, D., Mulcahy, J., Sellar, A., Walton, J., and Jones, C.: MOHC UKESM1.0-LL model output prepared for CMIP6 CMIP historical, https://doi.org/10.22033/ESGF/CMIP6.6113, 2019.